UNIVERSITY OF TURKU

QUANTUM PROBES FOR COMPLEX SYSTEMS

Francesco Cosco

UNIVERSITY OF TURKU

QUANTUM PROBES FOR COMPLEX SYSTEMS

Francesco Cosco

University of Turku

Faculty of Science and Engineering
Department of Physics and Astronomy

Supervised by

Sabrina Maniscalco
Department of Physics and Astronomy
University of Turku
Finland

Kalle-Antti Suominen
Department of Physics and Astronomy
University of Turku
Finland

Reviewed by

Mauro Paternostro
School of Mathematics and Physics
Queen's University Belfast
United Kingdom

John Goold
School of Physics
Trinity College Dublin
Ireland

Opponent

Anna Sanpera Trigueros
Departament de Física
Universitat Autònoma de Barcelona
Spain

Acknowledgements

Well, well, well. Look who finally decided to finish his thesis. How convenient. How ironic. How ironic, indeed.

It was a long journey from January 2015 when I first moved to Finland. During these years I had the luck of encountering many wonderful people along the way, both within and out of the University walls, and I apologise if I miss to include everyone in these few lines.

The first big thank goes without any shade of doubt to my supervisor Sabrina, who has warmly welcomed me in Turku almost four years ago. Thank you for guiding me along the way. Thanks to you I know what kind of physicist I want to be in the future. Thank you for the opportunities you gave me and for the blind trust you granted me in many occasions. I hope I have been up to the expectations.

I wish then to thank Kalle-Antti for all the work he has done for the University of Turku. Thank you in particular for the support you have been giving me, indirectly, supporting Sabrina in many situations.

A special thank goes then to Massimo, who has been present for me from the first stages of my Phd. Thank you for all the discussions we had and all the things we learned together. It goes without saying that a great part of this thesis work carries also your name.

It is then impossible to proceed without thanking all the amazing and smart people I had the chance to collaborate with during these years. I thank any single of them for sharing their knowledge with me and for all the interesting discussions we had. From you I learned how collaboration is the backbone of research. To you it goes my deepest gratitude.

Then, I thank all the occupants of the best room the laboratory of theoretical physics has ever seen, the infamous "noisy room". I thank past and current members for the nice working environment I had the possibility to work in. Thank you for all the wisdom that has been shared and for the high level of humour that has been *successfully* achieved during the years. Specifically, I thank Erkka, Mikko, Henri, Walter, and Jose for these

Contents

Abstract

Quantum probing is a fairly wide topic deepening its roots into many fields as it can borrow tools from, and be applied to, many-body physics, open quantum systems theory, quantum information and quantum thermodynamics. Its wide range of applicability, i.e. the diverse systems under investigations and their specific properties, contributes in making a general theory of quantum probing a rather challenging, if not impossible, task. Despite the need to specialize the probing technique to the various physical systems, we have identified a leitmotiv in our probing approach. Specifically, we will consider a perturbation potential acting as the source of the probing procedure, in most cases this will be an impurity in the complex environment acting as quantum probe. We will generally quantify the information exchange between the probe and its environment, and explore the connection to the concept of non-Markovian, i.e. memoryless, quantum dynamics.

This thesis aims at discussing probing protocols for atomic systems confined in optical lattices, both fermionic and bosonic species, as well as trapped ions. The systems inquired can be currently implemented in the field of ultra cold atoms, where they have attracted interest as ideal candidates for quantum simulators and quantum technologies. We will show how to design protocols in which these cold many-body systems act as an environment to a quantum probe, often designed as an impurity atom. Exploiting tools from open quantum systems theory we will discuss how to detect, from the dynamics of the probe, the characteristics of the complex environment.

The key idea is to use the quantum probe as read-out device, the properties of the environment are then inferred trough measurements performed exclusively on the probe. Quantities of interest will be related to the environment energy spectrum, equilibrium properties and temperature. The quantum probing paradigm will also allow us to investigate critical phenomena such as phase transitions and orthogonality catastrophe. Finally,

we will show how the memory effects induced in the reduced dynamics of an immersed quantum probe can witness, to some extent, the character of the excitations of the environment hinting to a natural link between non-Markovianity and localisation phenomena.

Tiivistelmä

Kvanttiluotaus on melko laaja aihepiiri joka juontaa juurensa moniin aloihin sillä se voi lainata menetelmiä, ja sitä voidaan soveltaa, monen kappaleen fysiikkaan, avoimien kvanttisysteemien teoriaan, kvantti-informaatioon ja kvanttitermodynamiikkaan. Sen laaja soveltuvuus, siis monet tutkimuksen alla olevat systeemit ja niiden erityiset ominaisuudet, tekevät yleispätevän kvanttiluotauksen teorian johtamisen melko haastavaksi, ellei peräti mahdottomaksi tehtäväksi. Siitä huolimatta, että luotaustekniikoiden on erikoistuttava kohteidensa mukaan, me olemme tunnistaneet omassa lähestymistavassamme johtoajatuksen. Tarkemmin sanottuna, me tarkastelemme häiriöpotentiaalia luotausmenetelmän välineenä. Useimmiten se tulee olemaan kompleksisen ympäristön epäpuhtaus, joka toimii kvanttiluotaimena. Yleisesti ottaen me kvantifioimme luotaimen ja ympäristön välisen informaationvaihdon, ja tutkimme sen yhteyttä ei-Markoviseen, siis muistittomaan, kvanttidynamiikkaan.

Tämä väitöskirja pyrkii käsittelemään luotausmenetelmiä sekä fermionisille että bosonisille atomisille systeemeille optisissa hiloissa, kuin myös loukutetuille ioneille. Käsiteltevien systeemien implementointi voidaan tällä hetkellä toteuttaa ultrakylmien atomien alassa, missä ne ovat herättäneet kiinnostusta kvanttisimulaattorien ja kvanttiteknologioiden ihanteellisina kandidaatteina. Me näytämme miten suunnitella menetelmiä missä nämä kylmät monen kappaleen systeemit toimivat ympäristönä kvanttiluotaimelle, jonka usein katsotaan olevan epäpuhtausatomi. Käyttäen hyväksi työkaluja avoimien kvanttisysteemien teoriasta me käsittelemme miten kompleksisen ympäristön luonteenomaiset ominaisuudet voi havaita luotaimen dynamiikasta.

Oleellinen ajatus on käyttää kvanttiluotainta mittarina josta ympäristön ominaisuudet voi lukea suorittamalla mittauksia yksinomaan luotaimelle. Kiinnostuksen kohteena olevat suureet liittyvät ympäristön energiaspektriin, tasapaino-ominaisuuksiin ja lämpötilaan. Kvanttiluotaamista käyttämällä voimme tutkia kriittisiä ilmiöitä kuten faasimuunnoksia ja or-

togonaalisuuskatastrofia. Lopuksi, me näytämme miten kvanttiluotaimen redusoituun dynamiikkaan indusoidut muistiefektit voivat osoittaa, tietyissä rajoissa, ympäristön eksitaatioiden luonteen, vihjaten luonnolliseen yhteyteen ei-Markovisuuden ja lokalisaatioilmiöiden välillä.

List of papers

This thesis consists of a review of the subject and the following original research articles: [1–8]:

I **Thermometry of ultracold atoms via non-equilibrium work distributions**,
   T. H. Johnson, *F. Cosco*, M. T. Mitchison, D. Jaksch, S. R. Clark, Phys. Rev. A **93**, 053619 (2016)

II **Momentum-Resolved and Correlations Spectroscopy Using Quantum Probes**,
   F. Cosco, M. Borrelli, F. Plastina, S. Maniscalco, Phys. Rev. A **95**, 053620 (2017)

III **Non-equilibrium quantum thermodynamics in Coulomb crystals**,
   F. Cosco, M. Borrelli, P. Silvi, S. Maniscalco, G. De Chiara, Phys. Rev. A **95**, 063615 (2017)

IV **Bose-Hubbard lattice as a controllable environment for open quantum systems**,
   F. Cosco, M. Borrelli, J. J. Mendoza Arenas, D. Jaksch, F. Plastina, S. Maniscalco, Phys. Rev. A **97**, 040101(R) (2018)

V **Statistics of orthogonality catastrophe events in localised disordered lattices**,
   F. Cosco, M. Borrelli, E.-M. Laine, A. Scardicchio, S. Pascazio, S. Maniscalco, New J. Phys. **20**, 073041 (2018)

VI **Memory effects in a quasi-periodic Fermi lattice**,
   F. Cosco, S. Maniscalco, Phys. Rev. A **98**, 053608 (2018)

VII **Irreversible Work and Orthogonality Catastrophe**,
   F. Cosco, arXiv:1809.01855 (2018)

VIII **Momentum-resolved spectroscopy of a 1D superfluid using a single atomic impurity**,
F. Cosco, M. Borrelli, F. Plastina, S. Maniscalco, arXiv:1811.01939 (2018)

Other published material

This is a list of the publications produced which have not been chosen as a part of this doctoral thesis

- **Entanglement Protection via Periodic Environment Resetting in Continuous Time Quantum Dynamical Processes**,
T. J. Bullock, *F. Cosco*, M. Haddara, S. Hamedani Raja, O. Kerppo, L. Leppäjärvi, O. Siltanen, N. W. Talarico, A. De Pasquale, V. Giovannetti, S. Maniscalco, Phys. Rev. A **98**, 042301 (2018)

- **Emergence of anomalous dynamics from the underlying singular continuous spectrum in interacting many-body systems**,
J. Settino, W. Talarico, *F. Cosco*, F. Plastina, S. Maniscalco, N. Lo Gullo, arXiv:1809.10524 (2018)

Introduction

A new technological era is upon us as the basic ingredients for a new generation of quantum technologies are currently being investigated and built in laboratories all over the world. We are on the verge of a new scientific and technological revolution that promises to affect profoundly research, technology and society at large. Therefore, developing innovative techniques for the control, manipulation and probing of such devices is clearly not only a technical necessity, but also a challenge of both applicative and fundamental nature.

A *probe* is, loosely speaking, a *device* that allows us to learn something about nature and the world around us. In a very broad sense we deal with such devices on a daily basis since centuries. It is sufficient to think about compasses, thermometers and so on. However, most probes we are familiar with usually are meant to measure macroscopic and classical quantities. The next quantum revolution requires instead a novel methodology, adequate and properly designed, to explore isolated quantum systems. These are the protagonists of current prototypes for quantum technologies. Differently from the classical case, measuring quantum systems generally perturbs and modifies their quantum states. Hence quantum probing presents different challenges but, perhaps, also new opportunities with respect to their classical counterpart. Of course, we should stress that a plethora of measurement techniques for extracting properties of isolated quantum systems exist but an interesting question naturally arises: can a probe of intrinsically quantum nature be more useful than usual measurement techniques? In a more general framework, we may also ask whether a *quantum probe*, mainly intended as a fully controllable component separated from the quantum system in exam, is able to unravel new insights about the properties of a complex quantum system to which it is coupled.

This novel approach has already found extensive applications when studying optically trapped cold atoms [9–11]. Various schemes and proposal, not limited to lattice gases, have been develop, such as, to mention

a few, to probe temperature [12], phononic excitations in bosonic systems [13], phonon dynamics in warm crystals [14], Luttinger physics [15], orthogonality catastrophe [16–20], Anderson localisation [21], the spectral properties of complex quantum networks [22], properties of squeezed thermal states [23], critical phenomena [24–26], and cutoff frequency of Ohmic environments [27]. In this pletora of applications it worth to mention how different types of quantum probes have been actually employed, such as quantum information probes [28], Feynman probes [29], entangled probes [30], and continuous-variable quantum probes [31].

The quantum probing paradigm assumed in this thesis relies on the full knowledge of the probe details as well as the full controllability of both its properties and its coupling with the system to be probed. In most cases the quantum probe will be modelled as an impurity atom and the inquired environment will be a system of trapped ultra-cold atoms, both bosons and fermions, particles and quasi-particles. The proposed protocols will investigate different sets of quantities ranging from areas of fundamental interest to more applicative ones. Focus will be put on protocols aimed at extracting information about thermal properties, spectral properties and critical phenomena.

The use of quantum probes is conceived as an alternative to more invasive traditional techniques and their possible use is justified by recent experiments with impurities immersed in optically trapped atomic gases where control over single atoms can be achieved [32–35].

The thesis is organised as follows. In Chapter 1, the basic theoretical tools to describe quantum probing protocols are introduced. Standard ingredients from open quantum system theory are presented, introducing the basic formalism for the time evolution of the probe that is treated as an open quantum system. The assumptions necessary to derive the master equation are discussed and it is shown that they are naturally justified when designing a probing protocol with the ultimate goal of being as less invasive as possible. The Breuer-Laine-Piilo non-Markovianity measure is then introduced and, throughout this thesis, it will be used as a criterion for quantifying non-Markovian dynamics and memory effects. As a paradigmatic example the dynamics of a two level system undergoing a purely decoherent evolution is then derived. In this particular case it is also shown how the information backflow can be calculated exactly. A different approach to quantum probing is presented in terms of the Fermi Golden Rule. The idea is to use a perturbative treatment to compute the

transitions between the energy levels of the probe induced by its coupling to the complex environment. At the end of Chapter 1, we will focus on some concepts needed to introduce probing of thermal, or quantum thermodynamical, properties. Specifically, we will introduce the formalism of the work distributions in relation to a quench of the total Hamiltonian. The fluctuation theorem known as Tasaki-Crooks relation is then presented and the concepts of average work and irreversible work production due to the quench are briefly discussed.

In Chapter 2 the physical systems used in our investigation, and for which the probing protocols have been proposed and tested, are presented. We first introduce bosonic models and then we describe the fermionic ones, although some of the protocols presented are independent from the specific environment. The first physical system presented is the one described by the Bose-Hubbard model. The transition from superfluid to Mott insulator is discussed along with the perturbative approaches available in literature, i.e. the Bogoliubov mean field theory for the superfluid phase and the doublon/holons description for the Mott insulator. The chapter proceeds discussing the physics of a system of trapped ions knowns as Coulomb Crystals and the structural phase transition they undergo when tuning the trapping fields. In an anisotropic trap, with weak trapping in the axial direction and strong trapping in the two transverse directions, two equilibrium configurations, namely a linear chain and a planar zig-zag structure, exist, depending on the relative value of the two transverse trapping frequency. In this scenario, the transverse frequency is acting as a critical parameter. We discuss the approximation that allow one to treat the model as a tight binding Hamiltonian and recast its description in terms of an effective short range model close to the criticality. Employing a further harmonic approximation the normal frequencies are presented. Due to the strong interaction the ions are effectively distinguishable particles and the fluctuations around the equilibrium positions can be quantized and described as bosonic excitations. We then proceed introducing fermionic tight binding models. The first one is an exactly solvable model represented by a generalisation of the Kitaev chain with long-range tunnelling. The second model is the so-called Aubry-André model which consists of a system of fermions trapped in a quasi periodic potential. Recently, this model has attracted a great deal of attention because of its unique features and the possibility of being realised in cold-atomic setups by means of two interfering optical lattices with incommensurate frequencies. The transition from delocalised

to exponentially localised single particle eigenstates, as a function of the quasi-periodic potential with a well defined critical point, makes this model an ideal platform to study localisation phenomena. This chapter is far from being a complete description of the aforementioned systems, it rather aims at being a self-consistent introduction about the physical systems for which the quantum probing protocols have been designed.

The following chapters contain an introductory overview of the probing protocols developed for the systems presented in Chapter 2. We begin by showing in Chapter 3 how a single weakly interacting controllable quantum probe can be used to perform full momentum-resolved spectroscopy of an environment with a lattice-like geometry. As a specific example, we apply this approach to show how to extract the dispersion relation of the Kitaev chain normal modes and of the phononic modes of a one-dimensional Bose-Hubbard lattice in the superfluid phase. We then discuss how, tracking the dynamics of an immersed impurity and controlling in time its coupling with a thermal environment, the temperature of the bath can efficiently extracted. This protocol relies on the measurement of the decoherence function of the probe, which can be used to infer temperature via the Crooks-Tasaki fluctuation theorem. The irreversible work produced during sudden infinitesimal quenches in proximity to the structural linear-zigzag transition of ion Coulomb Crystals is then discussed. We show how this quantity captures the critical properties of the model and can be extracted by local measurements on the ions. This chapter is an overview of the results of papers I, II, III and VIII.

The focus of the next chapter is the study of impurity-induced phenomena. More specifically, in Chapter 4 the results of papers IV and VI are presented and the probe dynamics is analysed from an open quantum systems theory perspective. In particular, the link between memory effects and localisation phenomena is explored. Our results show that, while the superfluid phase of the Bose-Hubbard system behaves as a Markovian environment for the probe, deep in the Mott insulator phase the rise of memory effects, signature of non-Markovian dynamics, can be witnessed. A subsequent result, complementing the one obtained for bosonic systems, allows us to conclude that memory effects are also witnessed in the metal to insulator transition for a system of fermions trapped in a quasi-periodic potential.

Chapter 5, finally, challenges the paradigm according to which an impurity weakly affects its environment. It is indeed dedicated to a detailed

study of the effects of local perturbations in the Aubry André model. New insight on the statistical orthogonality catastrophe are highlighted when the full statistics of orthogonality events is taken into account. We have indeed shown that, when scanning different energy scales for the impurity-fermions interaction, the properties of the Aubry-André spectrum manifest themself in a non trivial way in the full statistics of orthogonality events. To complete our investigation we explore a similar scenario focussing now on thermodynamic quantities. We show how the orthogonality catastrophe and the features of its statistics can be explained in terms of level crossings and avoided crossings, and how the latter ones are beautifully captured by the irreversible work production. This chapter contains the results of paper V and VII.

In the concluding remarks the key findings of the thesis are summarised and discussed in view of future investigations. The reader is assumed to be familiar with basic quantum mechanics, and its formulation in second quantisation.

Chapter 1

Quantum Probing: tools

The problem of designing efficient *quantum probing* protocol can be tackled in countless ways, and its optimization is generally system-specific. In several physical situations one does not have access to the full system and can only assume to be able to reliably model and control the coupling between the probe and the environment. One way to proceed is to study how the environment changes in response to a (usually sudden) variation of a system parameter, operation usually referred to as a *quench*, by measuring exclusively local components. The idea behind this approach is to infer through local measurements how the system reacts globally. This methodology, although effective in many cases, often requires a high level of knowledge about the inquired system and, therefore resulting sometimes impractical or unfeasible. An alternative way to proceed consists in considering the *quantum probe* as a separate object of which one has full controllability and complete knowledge. The probe is then coupled, for a certain time, to the environment (i.e. complex quantum system), which causes the former one to lose coherences. The properties of the environment are then mapped into the incoherent dynamics of the quantum probe and can then be indirectly measured by observing the probe, ideally, minimally disturbing the environmental state. In this approach the quantum probe acts as an actual read-out device.

1.1   Open Quantum Systems

Let us consider a system composed of two components in which one is identified as the probe, denoted as P, and the other one is identified as the environment, denoted as E. Without loss of generality we can assume that

the Hamiltonian of the total closed system $P + E$ can be written as

$$\hat{H} = \hat{H}_P + \hat{H}_E + g\hat{H}_{int}, \tag{1.1}$$

where $\hat{H}_P$ and $\hat{H}_E$ are the free Hamiltonians of the probe and of the environment, respectively. The last term is the interaction Hamiltonian between the probe and the environment and it is assumed to be proportional to a dimensionless coupling constant g. If the state of the total system at some initial time t_0 is described by a density operator $\hat{\rho}(t_0)$ the state at time t is then given by

$$\hat{\rho}(t) = \hat{U}(t, t_0)\hat{\rho}(t_0)\hat{U}^\dagger(t, t_0), \tag{1.2}$$

which is the formal solution to the Liouville-von Neumann equation

$$\frac{\mathrm{d}}{dt}\hat{\rho}(t) = -i\left[\hat{H}, \hat{\rho}(t)\right]. \tag{1.3}$$

This is the equation ruling the dynamics of the closed system and in the interaction picture reads

$$\frac{\mathrm{d}}{dt}\hat{\rho}(t) = -ig\left[\hat{H}_{int}(t), \hat{\rho}(t)\right]. \tag{1.4}$$

In most situations the dynamics of the total system is rather difficult if not impossible to calculate. However, in the spirit of quantum probing, our focus is on the dynamics of the probe, that then needs to be treated as an open system. By tracing out the degrees of freedom of the environment from (1.4) we get the following equation of motion for the reduced state of the probe

$$\frac{\mathrm{d}}{dt}\hat{\rho}_P(t) = -ig\mathrm{Tr}_E\left[\hat{H}_{int}(t), \hat{\rho}(t)\right]. \tag{1.5}$$

This equation, still exact, does not bring any concrete advantages. However, by following standard techniques we can recast the equation of motion of the probe in a more useful form. The first step is to insert into Eq. (1.5)

the integral form $\hat{\rho}(t) = \hat{\rho}(t_0) - ig \int_{t_0}^{t} \mathrm{d}s \left[\hat{H}_{int}(s), \hat{\rho}(s) \right]$ and obtain

$$\frac{\mathrm{d}}{dt}\hat{\rho}_P(t) = -ig \mathrm{Tr}_E \left[\hat{H}_{int}(t), \hat{\rho}(t_0) \right] - g^2 \int_{t_0}^{t} \mathrm{d}s \mathrm{Tr}_E \left[\hat{H}_{int}(t), \left[\hat{H}_{int}(s), \hat{\rho}(s) \right] \right].$$
(1.6)

In many physical situations $\mathrm{Tr}_E \left[\hat{H}_{int}(t), \hat{\rho}(t_0) \right] = 0$. Even when this is not the case, this term can be included in the unitary evolution prior to moving to the interaction picture. This allows one to further simplify the probe equation of motion as follows

$$\frac{\mathrm{d}}{dt}\hat{\rho}_P(t) = -g^2 \int_{t_0}^{t} \mathrm{d}s \mathrm{Tr}_E \left[\hat{H}_{int}(t), \left[\hat{H}_{int}(s), \hat{\rho}(s) \right] \right].$$
(1.7)

This equation is still exact, but it serves as the basis to further assumptions aimed at efficiently modelling the dynamics of an optimal quantum probe. Generally one desires a quantum probe to be least invasive and therefore it is reasonable to assume weak probe-environment coupling, in order to minimize the impact of the probe interaction on the environment. At the same time, prior to the probing protocol, it is reasonable to consider the probe and the environment initially factorised at time t_0. As a consequence of these two assumptions we can write

$$\hat{\rho}(t) \approx \hat{\rho}_P(t) \otimes \hat{\rho}_E.$$
(1.8)

This approximation is known as Born approximation and it has been employed widely in the field of open quantum system theory. In some cases, however, weak coupling cannot be assumed or strong interactions might be needed in order to reveal some specific properties of the environment. In such cases different approaches are needed. Inserting this approximation into Eq. (1.7) still leads to an integro-differential equation, therefore the next approximation consists in replacing $\hat{\rho}_P(s)$ with $\hat{\rho}_P(t)$. With this last approximation we finally arrive to the so-called Redfield equation

$$\frac{\mathrm{d}}{dt}\hat{\rho}_P(t) = -g^2 \int_{t_0}^{t} \mathrm{d}s \mathrm{Tr}_E \left[\hat{H}_{int}(t), \left[\hat{H}_{int}(s), \hat{\rho}_P(t) \otimes \hat{\rho}_E \right] \right].$$
(1.9)

This equation for the probe dynamics is local in time and in some cases can be analytically solved. Later in this chapter the paradigmatic example

of a qubit undergoing a pure dephasing dynamics will be discussed.

1.1.1   Memory effects: a definition of non-Markovianity

In many physical situations Eq. (1.9) can be further simplified by means of standard methods [36], i.e. making further approximations, namely the Markovian approximation and the rotating wave approximation. Under these assumptions one derives a master equation for the reduced dynamics in the so-called Lindblad form, i.e.

$$
\frac{\mathrm{d}}{dt}\hat{\rho}_P(t) = -i\left[\hat{H}_P, \hat{\rho}_P(t)\right] + \sum_k \gamma_k \left[\hat{A}_k\hat{\rho}_P(t)\hat{A}_k^\dagger - \frac{1}{2}\left\{\hat{A}_k^\dagger\hat{A}_k, \hat{\rho}_P(t)\right\}\right],
$$
(1.10)

where the coefficients $\gamma_k \geq 0$ are positive decay rates and $\hat{A}_k$ are known as jump or Lindblad operators. This equation is also known as GKSL equation, from Gorini, Kossakowski, Sudarshan and Lindblad who independently characterised the properties of Markovian master equations [37, 38]. A linear operator Λ_{t,t_0} which sends any initial open system state $\hat{\rho}_P(t_0)$ to the corresponding open system state $\hat{\rho}_P(t)$, i.e.

$$
\hat{\rho}_P(t_0) \mapsto \hat{\rho}_P(t) = \Lambda_{t,t_0}\hat{\rho}_P(t_0),
$$
(1.11)

is called a quantum dynamical map. When obtained as solution of the master equation Eq. (1.10) a dynamical map is complete positive and trace preserving (CPTP) and belongs to the Markov semi-group [39]. Maps belonging to this semi-group are characterised by time-homogeneity, i.e.

$$
\Lambda_{t,t_0} = \Lambda_{t-t_0,0} \equiv \Lambda_\tau,
$$
(1.12)

where $\tau = t - t_0$, and by the semi-group property

$$
\Lambda_{t_1+t_2} = \Lambda_{t_1}\Lambda_{t_2}.
$$
(1.13)

Loosely speaking the concept of memoryless (Markovian) dynamics can be associated to this property of the dynamical map, namely the fact that it can be written as a concatenation of infinitely many dynamical maps describing the time evolution of each inifinitesimal time-step increment. This concept can be further generalised to the case in which the decay rates

in Eq. (1.10) are time dependent but positive at each time, i.e $\gamma_k(t) \geq 0$ for every t. In this case it is found that the dynamical maps satisfy the so-called divisibility property, namely

$$\Lambda_{t,t_0} = \Lambda_{t,\tau}\Lambda_{\tau,t_0}, \qquad (1.14)$$

where the propagator $\Lambda_{t,\tau}$ is completely positive. Any open quantum dynamics obtained as solution of the master equation of Eq. (1.10) or possessing the divisibility property of Eq. (1.14) is commonly referred to as *Markovian*. In the last few years many measures or witnesses of non-Markovianity, based on different properties, have been proposed and employed in the attempt to give a more transparent physical interpretation of memory effects. Generally, different non-Markovianity measure are not equivalent and hierarchies of such measures, as well as different degrees of non-Markovianity, have been studied in the literature [40–45]. In this thesis we follow the framework set by Breuer, Piilo and Laine (BLP) which identifies non-Markovianity, and specifically memory effects, with the presence of information backflow [46, 47]. The BLP measure is built considering how the distinguishability between two quantum states evolves in time under the effect of the dynamical map describing the open system evolution. The distinguishability is defined trough the trace distance that, for two generic quantum states $\hat{\rho}_1$ and $\hat{\rho}_2$, reads as

$$D\left[\hat{\rho}_1, \hat{\rho}_2\right] \equiv \frac{1}{2}\text{Tr}\sqrt{(\hat{\rho}_1 - \hat{\rho}_2)(\hat{\rho}_1 - \hat{\rho}_2)}. \qquad (1.15)$$

It has been proven that the distinguishability between any pair of states, quantified by the trace distance, is contractive under any completely positive and trace preserving map. Formally speaking

$$D\left[\hat{\rho}_1(t_1 + \tau), \hat{\rho}_2(t_2 + \tau)\right] \leq D\left[\hat{\rho}_1(t_1), \hat{\rho}_2(t_2)\right]. \qquad (1.16)$$

This implies that for divisible dynamical maps the distinguishability between states continuously and monotonically decreases as a function of time. Hence, an increase in trace distance signals the lack of divisibility, i.e. non-Markovianity. Within this framework the intervals of time in which the distinguishability decreases are associated with information flowing from the system to the environment, while during the intervals in which the trace distance temporarily increases we witness information com-

ing back to the system, i.e. information backflow and memory effects. The BLP non-Markovianity measure, or information backflow, is then defined and quantified as follows

$$\mathcal{N}_- [\Lambda] = \max_{\rho_{1,2}(0)} \int_{\dot{D}>0} dt \left[\frac{d}{dt} D \left[\Lambda_t \hat{\rho}_1(0), \Lambda_t \hat{\rho}_2(0) \right] \right]. \qquad (1.17)$$

According to this definition to classify a quantum dynamical map as non-Markovian one should be able to carry out the optimisation process over all pairs of possible initial states. Clearly this is in general a rather challenging task, but an analytical expression can be derived for certain dynamical maps. In the same fashion it can be useful to quantify the information outflow, i.e. the information lost to the environment, in an analogous way

$$\mathcal{N}_+ [\Lambda] = \max_{\rho_{1,2}(0)} \int_{\dot{D}<0} dt \left[\frac{d}{dt} D \left[\Lambda_t \hat{\rho}_1(0), \Lambda_t \hat{\rho}_2(0) \right] \right]. \qquad (1.18)$$

1.1.2   Pure Dephasing: single qubit

One of the simplest types of evolution for the open dynamics of a two level system is, without any doubt, the pure dephasing. This consists of an evolution dynamics that affect exclusively the coherences of the system in the basis in which it has been derived. Let us call the two levels $|g\rangle$ and $|e\rangle$. The reduced density matrix of the two level system obeys a master equation of the form

$$\frac{\mathrm{d}}{dt} \hat{\rho}_P(t) = \gamma(t) \left[\sigma_Z \hat{\rho}_P(t) \sigma_Z - \hat{\rho}_P(t) \right]. \qquad (1.19)$$

The specifics of the interaction and/or the information about the the environment are encoded into the dephasing rate $\gamma(t)$. If a microscopic derivation is possible, such as for an interaction Hamiltonian of the form $g\hat{H}_{int} = |e\rangle\langle e| \otimes \hat{V}$, which we will consider later in this thesis, then the solution of the master equation of Eq. (1.9) leads to the equation

$$\frac{\dot{\chi}(t)}{\chi(t)} = -g^2 \int_0^t \mathrm{d}s \mathrm{Tr}_E \left[\hat{V}(t)\hat{V}(s)\hat{\rho}_E \right], \qquad (1.20)$$

where $\chi(t)$ is the decoherence function and it is related to the decay rate as $\dot{\chi}(t) = \gamma(t)$. The formal solution of the master equation can be written

in terms of a dynamical map Λ_t defined as

$$\hat{\rho}_P(t) = \Lambda_t[\hat{\rho}_P(0)] = \begin{pmatrix} \rho_{gg}(0) & \chi^*(t)\rho_{ge}(0) \\ \chi(t)\rho_{eg}(0) & \rho_{ee}(0) \end{pmatrix}. \qquad (1.21)$$

In some cases the decoherence function obtained by solving (1.20) coincides with the exact solution that one would get by solving and deriving the unitary evolution for the total system plus environment (1.21):

$$\chi(t) = \mathrm{Tr}\left\{\hat{\rho}_E(t_0)\mathcal{T}\exp[-\mathrm{i}\int_{t_0}^{t}\mathrm{d}\tau\hat{V}(\tau)]\right\} \qquad (1.22)$$

where $\mathcal{T}$ is the time-ordering operator. For this class of open dynamics the sign of the dephasing rate uniquely determines whether the dynamics is Markovian or non-Markovian. The dephasing dynamics for a two level system is one of the few cases in which the maximisation over the optimal pair of states in (1.17) can be carried out analytically [47, 48]. It is found that the optimal pair of states satisfies the conditions: $(\hat{\rho}_1(0)-\hat{\rho}_2(0))_{gg} = 0$ and $|(\hat{\rho}_1(0) - \hat{\rho}_2(0))_{eg}|^2 = 1$. With this pair it is straightforward to show that the optimised trace distance is given by the absolute value of the decoherence function

$$D_{opt}(t) = |\chi(t)|. \qquad (1.23)$$

We can therefore express the information backflow, combining Eq. (1.17) and Eq. (1.23), as

$$\mathcal{N}_- = \sum_n |\chi(t_{2n})| - |\chi(t_{1n})|, \qquad (1.24)$$

where $[t_{1n}, t_{2n}]$ are the time intervals over which $|\chi(t)|$ increases. Memory effects are then associated with a revival in the coherences of the system. Summing instead over the time intervals in which $|\chi(t)|$ decreases we can quantify also the information outflow $\mathcal{N}_+$. In the following we will also consider a normalised version of the BLP non-Markovianity measures, defined as the ratio between the information backflow and the information outflow,

as following:

$$\mathcal{R} = \frac{\mathcal{N}_-}{\mathcal{N}_+}. \tag{1.25}$$

1.2 Fermi Golden Rule

So far we have considered the possibility of following the dynamics of the probe in time by solving a master equation, might it be Markovian or non-Markovian. In many cases, however, the complexity of the interaction itself or of the probe free structure may suggest a different and more appropriate approach. We can model a very general quantum probe as a quantum system with a certain number of discrete energy levels

$$\hat{H}_P = \sum_{\bar{n}} \epsilon_{\bar{n}} |\bar{n}\rangle\langle\bar{n}| \tag{1.26}$$

where $\epsilon_{\bar{n}}$ are the probe free eigenenergies. Once again we consider a factorised state as initial state of the system $P + E$

$$\hat{\rho}(t_0) = \hat{\rho}_P(t_0) \otimes \hat{\rho}_E(t_0), \tag{1.27}$$

and assume that the initial state of the probe is a pure state $\hat{\rho}_P = |\bar{g}\rangle\langle\bar{g}|$, with $|\bar{g}\rangle$ being an eigenstate of the probe free Hamiltonian $\hat{H}_P$. Switching on the coupling between probe and environment at time t_0, and assuming the interaction $g\hat{H}_{int}$ to be weak, we can calculate the transition rates of the probe using a perturbative approach. The idea is to calculate, as a function of time, the probability of finding the probe in a different eigenstate, say $|\bar{e}\rangle$. Formally speaking this is equivalent to compute

$$\Gamma_{\bar{g}\to\bar{e}}(t) = \text{Tr}_E\left\{\langle\bar{e}|\hat{\rho}(t)|\bar{e}\rangle\right\} = \text{Tr}_E\left\{\langle\bar{e}|\hat{U}(t,t_0)\hat{\rho}(t_0)\hat{U}^\dagger(t,t_0)|\bar{e}\rangle\right\}, \tag{1.28}$$

where $\hat{U}(t,t_0)$ is the time evolution operator in the interaction picture. The assumption of weak coupling allows us to resort to an expansion in powers of g for the time evolution operator. We can make the following expansion $\hat{U}(t) = 1 + g\hat{U}_1(t) + g^2\hat{U}_2(t) + ...$ and truncate up to the first order in g. The relevant term considered in the transition rate is then

$\hat{U}_1(t) = -i \int_0^t dt_1 \hat{H}_{int}(t_1)$ and (1.28) reads

$$\Gamma_{\bar{g} \to \bar{e}}(t) \simeq g^2 \text{Tr}_E \left\{ \langle \bar{e}| \hat{U}_1(t)\rho(0)\hat{U}_1^\dagger(t)|\bar{e} \rangle \right\} + O(g^4)$$

$$= g^2 \int_0^t dt_1 dt_2 \text{Tr}_E \left\{ \langle \bar{e}| \hat{H}_{int}(t_1)\rho(0)\hat{H}_{int}(t_2)|\bar{e} \rangle \right\} + O(g^4). \quad (1.29)$$

In the weak coupling regime this expression works very well as its first correction would be of fourth order in g. Eq. (1.29) is the open quantum system equivalent of the Fermi Golden Rule [49, 50].

1.3 Quantum Thermodynamics

In the previous sections we have analysed the effect of the probe-environment coupling by tracking either the probe dynamics or the transitions induced among its energy levels. However, we can address the quantum probing problem from a different perspective. Focusing only on the environment let us write its time dependent Hamiltonian as

$$\hat{H}(t) = \hat{H}_E + g(t)\delta\hat{H}. \quad (1.30)$$

The basic idea is to imagine a scenario in which the Hamiltonian of the environment is temporarily modified and the control is now on the extra term $g(t)\delta\hat{H}$. The action of modifying the Hamiltonian ruling the dynamics of a quantum system is commonly known as a *quench*. The study of quench dynamics is a fairly fertile field and we now focus on its thermodynamic interpretation. We consider the case in which two sets of energy projective measurements are performed, the first at time t_0 and the second at time t_f. At time t_0 we project on the eigenstates of $\hat{H}(t_0) = \hat{H}_E$, with $\hat{H}(t_0)|n\rangle = E_n|n\rangle$, and at t_f on the eigenstates of $\hat{H}(t_f) = \hat{H}_E + g\delta\hat{H}$, where $g = g(t_f)$ and $\hat{H}(t_f)|n\rangle = E_{\bar{m}}|\bar{m}\rangle$. The distribution built by averaging over all possible outcomes, weighted with the probabilities related to the outcomes of both projective measurements, is then given by

$$P(W) \equiv \sum_{n,\bar{m}} p_n(t_0) p_{\bar{m}|n}(t_f)\delta\left(W - E_{\bar{m}} + E_n\right), \quad (1.31)$$

where $p_n(t_0) = \langle n|\hat{\rho}_E(t_0)|n\rangle$ is the probability of measuring E_n at time t_0, and $p_{\bar{m}|n}(t) = |\langle n|\hat{U}(t_f)|\bar{m}\rangle|^2$ is the conditional probability related to a

measurement of $E_{\bar{m}}$ at t_f assuming E_n as a result of the first measurement. Taking the environment to be initially in a thermal state $\hat{\rho}_E(t_0) = e^{-\beta \hat{H}_E}/\mathcal{Z}$ the probability associated to outcome E_n is simply $p_n(t_0) = e^{-\beta E_n}/\mathcal{Z}$. The function in Eq. (1.31) is known as work distribution as it introduces the concept of work in the quantum framework as energy difference between two projective measurements performed respectively before and after the quench [51]. One of the main results of the work distribution formalism is the Crooks-Tasaki fluctuation theorem that is built which connects two quenching protocols labelled as *forward* and *backward*. [52, 53] Labelling the protocol introduced above as forward, the backward one is defined by $\hat{H}(t_0) = \hat{H}_E + g\delta\hat{H}$, $\hat{H}(t_f) = \hat{H}_E$, where we assume $\hat{\rho}_E(t_0) = e^{-\beta(\hat{H}_E + g\delta\hat{H})}/\mathcal{Z}$. One can prove that

$$\frac{P_F(W)}{P_B(-W)} = e^{-\beta(W-\Delta F)}, \tag{1.32}$$

where F and B indicate the forward and backward work distributions, respectively, and ΔF is the free energy difference between two equilibrium configurations. Instead of calculating directly the work probability distributions of Eq. (1.31) it is often more feasible to compute its Fourier transform, namely the characteristic or moment-generating function

$$\chi_F(t) = \int dW e^{iWt} P_F(W) = \text{Tr}_E \left\{ e^{i\hat{H}(t_f)t} \hat{U}^\dagger(t_f) e^{-i\hat{H}(t_0)t} \hat{U}(t_f) \rho_E(t_0) \right\}. \tag{1.33}$$

From the characteristic function one can easily calculate the average work associated with the quench

$$\langle W \rangle = -i \frac{\partial \ln \chi_F(t)}{\partial t}\bigg|_{t=t_0}, \tag{1.34}$$

and its statistical variance

$$\sigma_W^2 = \langle W^2 \rangle - \langle W \rangle^2 = (-i)^2 \frac{\partial^2 \ln \chi_F(t)}{\partial t^2}\bigg|_{t=t_0}. \tag{1.35}$$

When studying quantum phase transitions it is useful to consider the irreversible work which is defined as the difference between the work produced

by the quench and the free-energy difference

$$W_{irr} = \langle W \rangle - \Delta F. \tag{1.36}$$

The quantity in Eq. (1.36) quantifies the deviation from a reversible and isothermal process and, at zero temperature, can be also interpreted as the energetic cost of the adiabatic deviation of a sudden quench [54]. Interestingly, it is possible, at finite temperature, to express the irreversible work in terms of the cumulants k_n of the work distribution, i.e.

$$W_{irr} = \sum_{n=2} (-1)^n \frac{\beta^{n-1}}{n!} k_n, \tag{1.37}$$

where the cumulants can be calculated from the characteristic function as $k_n = (-i)^n \frac{\partial^2 \ln \chi_F(t)}{\partial t^n}\Big|_{t=t_0}$. If the work distribution is gaussian, and in linear response regime, Eq. (1.37) can be further simplified and the irreversible work is found to be proportional to the variance of the work distribution, i.e. $W_{irr} = \beta \sigma_W^2 / 2$ [55, 56].

Chapter 2

Many-Body Systems

The quantum probing paradigm can be addressed in many ways and its range of applicability is quite vast as well. In this thesis we focus our attention on quantum probing protocols designed to inquire features and properties of quantum complex systems of interest for the development of quantum simulators and quantum technologies. The systems that we investigate can be all described by means of tight-binding Hamiltonians. These are theoretical models initially introduced to describe the dynamics of electrons in solids which, however, in recent years have been used to describe also cold atomic systems as the latter ones are ideal quantum simulators of a number of condensed matter systems. Despite the apparent simplification allowed by tight-binding Hamiltonians, we will show how complex phenomena can nonetheless arise from this description, such as phase transitions and other critical phenomena.

2.1 Bosonic Systems

2.1.1 Bose-Hubbard model

The Bose-Hubbard model is without any doubt the most celebrated tight-binding Hamiltonian. It has been proven to describe very well the dynamics of a one-dimensional gas of cold bosonic atoms trapped in an optical lattice and confined to the lowest Bloch band [57–60]:

$$\hat{H}_{BH} = -J \sum_{i=1} (\hat{a}_{i+i}^\dagger \hat{a}_i + \hat{a}_i^\dagger \hat{a}_{i+1}) + \frac{U}{2} \hat{n}_i(\hat{n}_i - 1), \qquad (2.1)$$

where J is the hopping parameter describing the mobility of the bosons in the lattice, U is the local on-site interaction between the bosons, $\hat{a}_i, \hat{a}_i^\dagger$ are the standard boson annihilation and creation operators, and $\hat{n}_i = \hat{a}_i^\dagger \hat{a}_i$ is the local number operator.

In the two trivial limits $J = 0$ and $U = 0$, the above Hamiltonian is easily solved, in the Fock space, i.e. in the occupation number basis, or momentum space respectively. The two ground states describe then a Mott insulator, with a uniform occupation number per site, or a quasi-condensate, with a macro-occupancy of the lowest momentum-state. For non zero hopping but in the limit of infinite interaction the system consists of the so-called hard-core bosons [61, 62] and can be mapped to a a system of free fermions and a number of analytical results can be derived. However, at intermediate interaction the model is analytically intractable and in the last few years many approximate models to describe the regimes in which $J \gg U$ and in which $U \gg J$ have been proposed and successfully employed.

The case in which $U \ll J$ is the regime known as superfluid phase and corresponds to the case in which the kinetic energy of the atoms in the lattice is dominant over the on-site interaction, and hence the latter can be treated as a weak perturbation. The gas is a 1D quasi-condensate whose majority of atoms occupy the $k = 0$ momentum state. In this regime one can employ Bogoliubov mean-field theory and replace the creation and annihilation operators $\hat{a}_{k=0}^\dagger$ and $\hat{a}_{k=0}$ with $\sqrt{N_0}$ [63]. Expanding the Hamiltonian and keeping exclusively the terms proportional to the macroscopic occupation we get

$$\hat{H} \simeq \frac{N_0^2 U}{2 N_s} + \sum_{k \neq} (\epsilon_k + 2n_0 U) \hat{a}_k^\dagger \hat{a}_k + \frac{n_0 U}{2} \sum_{k \neq 0} \hat{a}_k^\dagger \hat{a}_{-k}^\dagger + \hat{a}_k \hat{a}_{-k}, \qquad (2.2)$$

where N_s is the number of lattice sites, $n_0 = N_0/N_s$ is the condensate density, ϵ_k is the interaction-free particle energy which, for a square lattice in $1D$, is $\epsilon_k = 2J - 2J \cos(k)$. The Hamiltonian in Eq. (2.2) can be diagonalised trough a Bogoliubov transformation. The new modes are related to the creation and annihilation of original bosons in the momentum space by the following relations:

$$\hat{b}_k = u_k \hat{a}_k - v_k \hat{a}_{-k}^\dagger \qquad (2.3)$$

where u_k, v_k are the Bogoliubov coefficients [64–66]. With these the Hamil-

tonian (2.2) takes the form

$$\hat{H} \simeq \sum_k \omega_k \hat{b}_k^\dagger \hat{b}_k, \tag{2.4}$$

where the frequency of the normal modes is given by $\omega_k = \sqrt{\epsilon_k^2 + 2n_0 U \epsilon_k}$. For low values of the crystal momentum this system has a phononic dispersion relation, i.e. $\omega_k \simeq c_s k$, with sound speed $c_s = \sqrt{2JUn_0}$. Within this framework the local number operator is approximated as

$$\hat{n}_i \simeq n_0 + \frac{\sqrt{N_0}}{N_s} \sum_{k \neq 0} (\hat{a}_k^\dagger + \hat{a}_k). \tag{2.5}$$

The strongly interacting case $U \gg J$ requires a different approach where the hopping term is the perturbative parameter. A successful approximate theoretical description can be obtained truncating the local basis of each lattice site to the three states $\{|\bar{n}\rangle, |\bar{n} \pm 1\rangle\}$, with $\bar{n}$ the lattice filling factor [67]. The key idea is that in the strongly interacting case the ground state has the form $|GS\rangle \propto \otimes_j |\bar{n}\rangle_j$ and hence only the excited states $|\bar{n}+1\rangle, |\bar{n}-1\rangle$ play a major role as corrections. Following [67], within this basis, we can introduce a family of auxiliary flavoured bosons $\hat{b}_{j,\pm}$ related to the initial ones by

$$\hat{a}_j = \sqrt{\bar{n}+1}\, \hat{b}_{j,+} + \sqrt{\bar{n}}\, \hat{b}_{j,-}^\dagger. \tag{2.6}$$

The two flavours $\pm$ correspond to the creation of an excess or the lack of particles, namely $\hat{b}_{j,\pm}^\dagger |\bar{n}\rangle = |\bar{n} \pm 1\rangle$. Since they obey bosonic commutation relations more than one auxiliary boson can occupy a single site. Therefore, the hardcore constraint needs to be imposed and double occupancies of different species need to be eliminated. This amounts at imposing in the following conditions

$$(b_{j,\pm})^2 = (b_{j,\pm}^\dagger)^2 = 0, \tag{2.7a}$$

$$\hat{b}_{j,+}^\dagger \hat{b}_{j,+} \hat{b}_{j,-}^\dagger \hat{b}_{j,-} = 0. \tag{2.7b}$$

The next step is to perform the Jordan-Wigner transformation [68] in order to pass from a bosonic description to a fermionic one, that naturally will

obey to the condition imposed by Eq. (2.7a). These new fermionic modes are related to the old ones via the following relations

$$\hat{b}_{j,\pm} = Z_{j,\pm} \, \hat{f}_{j,\pm}, \tag{2.8}$$

where $Z_{j,\pm}$ are the chain operators ensuring that the new modes obey to anticommutation relations. The local number operator expressed in terms of these fermionic excitations is given by

$$\hat{n}_j = \bar{n} + \hat{n}_{j,+} - \hat{n}_{j,-}. \tag{2.9}$$

These new modes allow us to recast the Hamiltonian in the form

$$
\begin{aligned}
\hat{H} = \sum_j \mathcal{P} \Big\{ & -J(\bar{n}+1)\hat{f}_{j,+}^\dagger \hat{f}_{j+1,+} - J\bar{n}\hat{f}_{j+1,-}^\dagger \hat{f}_{j,-} \\
& - J\sqrt{\bar{n}(\bar{n}+1)}(\hat{f}_{j,+}^\dagger \hat{f}_{j+1,-}^\dagger - \hat{f}_{j,-}\hat{f}_{j+1,+}) + \text{H.c.} \\
& + \frac{U}{2}(\hat{n}_{j,+} - \hat{n}_{j,-}) \Big\} \mathcal{P}.
\end{aligned}
\tag{2.10}
$$

The projector $\mathcal{P} = \prod_j (1 - n_{+j}n_{-j})$ is introduced to formally take into account the constraint imposed by Eq. (2.7b). This description in terms of fermionic excitations can be further simplified imposing the unconstrained fermions approximation, which consists in taking $\mathcal{P} \to 1$. This approximation is justified by the fact that the mechanism leading to the creation of double occupancies is a local pairing which is suppressed by the fermionic particles statistics. Furthermore, in [67] it is shown how the validity of this approximation is enhanced for increasing interaction. Within this limit the Hamiltonian is quadratic and once in the momentum space can be exactly diagonalised by means of a Bogoliubov transformation

$$\hat{H} \simeq \sum_k \omega_k^d \hat{d}_k^\dagger \hat{d}_k + \omega_k^h \hat{h}_k^\dagger \hat{h}_k, \tag{2.11}$$

where, for $\bar{n} = 1$, the creation and annihilation operators $\hat{d}_k^\dagger, \hat{d}_k$ are the doublon mode fermionic Bogoliubov operators, and $\hat{h}_k^\dagger, \hat{h}_k$ are the holon fermionic Bogoliubov operators. The quasi-particle excitations spectrum reads $\omega_k^{d/h} = \mp J\cos k + \Omega_k$, with $\Omega_k = \sqrt{(E_k^+ + E_k^-)^2 + 4|\Delta_k|^2}/2$, with $E_k^\pm = -2J(\bar{n} + \frac{1}{2} \pm \frac{1}{2})\cos k + U/2$ and $\Delta_k = 2iJ\sqrt{\bar{n}(\bar{n}+1)}\sin k$. These

modes are obtained through the following transformations

$$\hat{d}_k = \cos\theta_k \hat{f}_{k,+} + \mathrm{i}\sin\theta_k \hat{f}^\dagger_{-k,-},$$
$$\hat{h}_k = \cos\theta_k \hat{f}^\dagger_{k,-} - \mathrm{i}\sin\theta_k \hat{f}^\dagger_{-k,+},$$

(2.12)

where the Bogoliubov angles are $\theta_k = \arctan\left[-2i\Delta_k/(E_k^d + E_k^h)\right]$. This theory is known to break down for $U/J < 4(\bar{n}+1)$, therefore choosing $\bar{n} = 1$ restricts the range of validity to $U/J > 8$.

2.1.2 Coulomb Crystals

Trapped and mutually repelling ions are a unique platform with a rich physics determined by the interplay between the trapping potential and the Coulomb interaction [69]. In particular, ions confined in anisotropic traps and interacting via a repulsive Coulomb interaction undergo a structural phase transition in which their spatial geometry changes. In an ion trap with strong transverse trapping and weaker axial confinement the most favourable energy configuration is given by a linear chain. However, when reducing the transverse trapping frequency, the favourable energy configuration is a planar zig-zag configuration. This is a structural phase transition in which the frequency of the transverse harmonic trapping potential is the parameter driving the transition [70]. The Hamiltonian for a system of trapped ions in first quantization can be written as

$$\hat{H} = \sum_{j=1}^{L}\left[\frac{\hat{P}_{x,j}^2 + \hat{P}_{y,j}^2}{2M} + \frac{M\omega_0^2}{2}\hat{Y}_j^2 + V_L(\hat{X}_j)\right]$$
$$+ \frac{Q^2}{8\pi\epsilon_0}\sum_{i\neq j}\left[(\hat{X}_i - \hat{X}_j)^2 + (\hat{Y}_i - \hat{Y}_j)^2\right]^{-1/2}$$

(2.13)

where Q is the ion charge, M the mass, $(\hat{X}_j, \hat{Y}_j)$ and $(\hat{P}_{x,j}, \hat{P}_{y,j})$ the position and momentum operators of the $j-$th ion respectively, and $V_L(x)$ is the longitudinal component of the confining potential. We have assumed the repulsion to be strong enough to treat the ions as distinguishable particles. We have also neglected the motion in the z direction since our focus is on the linear to planar zig-zag transition. The quantum nature of this model rely on the canonical commutation relations $[X_i, P_{x,j}] = [Y_i, P_{y,j}] = i\hbar\delta_{ij}$. It can be shown that, close to criticality, the longitudinal and transversal

components in Eq. (2.13) effectively decouple [71, 72]. One can therefore fix the average equilibrium positions of the ions along the longitudinal direction to $x_j = ja$, with a being the effective lattice spacing, and write for the transverse motion

$$\hat{H}_y = \sum_{j=1}^{L} \left[\frac{\hat{P}_{y,j}^2}{2M} + \frac{M\omega_0^2}{2}\hat{Y}_j^2 \right] + \frac{Q^2}{8\pi\epsilon_0} \sum_{i \neq j} \left[a^2(i-j)^2 + (\hat{Y}_i - \hat{Y}_j)^2 \right]^{-1/2}.$$
(2.14)

Furthermore, the Coulomb term of the transverse Hamiltonian H_y can be Taylor-expanded in the transverse displacements, which, close to the transition point, are much smaller than the inter-ions distance. The resulting Hamiltonian can then be recast into a short-range model through an expansion of the scattering matrix of the harmonic modes to second order in δk around the soft mode ($\delta k = k - \pi/a$), which is dominant close to the critical point [73]. This procedure allows us to simplify the Hamiltonian (2.14) leading to the following form

$$\frac{\hat{H}_y}{E_0} = \frac{1}{2} \sum_{j=1}^{L} \left[-g^2 \frac{\partial^2}{\partial y_j^2} + (\omega^2 - h_1)\hat{y}_j^2 + h_2(\hat{y}_j + \hat{y}_{j+1})^2 + h_3\hat{y}_j^4 \right],$$
(2.15)

which is a dimensionless Hamiltonian obtained dividing by $E_0 = Q^2/(4\pi\epsilon_0 a)$. In Eq. (2.15) $y_j = Y_j/a$, $\omega = \omega_0/\sqrt{E_0/Ma^2}$, $h_1 = 7\zeta(3)/2$, $h_2 = \ln 2$, $h_3 = 93\zeta(5)/8$, with ζ being the Riemann function, and $g = \sqrt{\hbar^2/Ma^2 E_0}$ plays the role of an effective Planck constant quantifying the impact of quantum fluctuations [74, 75]. For small quantum fluctuations the dynamics of the ion crystal can be expressed in terms of small quantum displacements, coupled harmonically, around the classical equilibrium ion positions. In the linear phase the classical equilibrium positions are $y_j = 0$ while in the zigzag phase these are $y_j = (-1)^j b/2$ where the zigzag width b is determined by ω. In this regime one can find easily the normal frequencies of the chain. In the linear phase these read

$$\omega_k^2 = g^2 \left[\omega^2 - h_1 + 4h_2 \cos^2 \frac{k}{2} \right]$$
(2.16)

This semiclassical model predicts a critical transverse frequency at $\omega_C = \sqrt{h_1}$, for which the frequency of the soft-mode at $k = \pi$ vanishes. For

$\omega > \omega_C$ the chain spatial configuration is linear, while it is zig-zag in the opposite case. When considering the full quantum model, without approximating the anharmonic term, one finds that the critical point can be computed as a function of g, and it was estimated to scale as $\omega_C(g) \approx h_1 - 3h_3 g |\ln g| / 2\pi + \mathcal{O}(g)$ for small values of g. In this sense the effective Planck constant causes a shift of the critical point.

2.2 Fermionic Systems

2.2.1 Kitaev model

The Kitaev chain is a tight-binding model which describes a p-wave super-conducting wire that, under certain conditions has a gapped bulk together with zero-energy unpaired Majorana modes localized at the edges of the system. In the past few years many variants and generalisation of this model have been proposed. Here, we consider a generalized Kitaev chain with long-range hopping, nearest neighbours pairing [76, 77], and periodic boundary conditions with Hamiltonian given by

$$\hat{H} = \sum_{l \neq j = 1}^{N_s} J_{lj} \hat{a}_l^\dagger \hat{a}_j + \Delta \sum_{j=1} \hat{a}_j^\dagger \hat{a}_{j+1}^\dagger + \text{H.c.}, \qquad (2.17)$$

where Δ and $J_{lj} = J|\pi/(N_s \sin[\pi(l-j)/N_s])|^\alpha$ are the pairing and long range tunnelling coefficients, respectively. Long-range hopping models such as (2.17) have been receiving renewed attention due to their shared features with long-range Ising models [78], and the possible experimental realisability with ultracold neutral atoms and trapped ions simulators [79–81]. In the momentum space the Hamiltonian can be written as

$$\hat{H} = \sum_k J(k) \hat{a}_k^\dagger \hat{a}_k + 2i\Delta \sin(k) \hat{a}_k^\dagger \hat{a}_{-k}^\dagger + \text{H.c.}, \qquad (2.18)$$

where $J(k) = \sum_d J_{j,j+d} \cos(k)$. The Kitaev Hamiltonian is quadratic and therefore is easily diagonalised by means of Bogoliubov transformations. The Bogoliubov modes are obtained trough the following relations

$$\hat{c}_k = \cos(\theta_k/2) \hat{a}_k^\dagger - i \sin(\theta_k/2) \hat{a}_{-k}, \qquad (2.19)$$

where θ_k are the Bogoliubov angles and satisfy the equation

$$e^{i\theta_k} = \frac{J(k) + 2i\Delta \sin(k)}{\sqrt{J^2(k) + 4\Delta \sin^2(k)}}. \tag{2.20}$$

Recasting Eq. (2.17) in terms of the Bogoliubov modes, leads to its diagonal form

$$\hat{H} = \sum_k \omega_k \hat{c}_k^\dagger \hat{c}_k, \tag{2.21}$$

with the quasiparticle spectrum given by $\omega_k = \sqrt{J^2(k) + 4\Delta \sin^2(k)}$.

2.2.2 Aubry-André model

Similarly to the case of the Bose-Hubbard model previously introduced, a one-dimensional gas of fermions trapped in an optical lattice is well described by the Fermi-Hubbard Hamiltonian [82–84]. When the particles are trapped in a dichromatic optical lattice the Hamiltonian describing for a system of non interacting spinless fermions is given by

$$\hat{H} = -J \sum_{i=1}(\hat{a}_{i+i}^\dagger \hat{a}_i + \hat{a}_i^\dagger \hat{a}_{i+1}) + \Delta \sum_{i=1} \hat{n}_i \cos(2\pi\beta i + \phi), \tag{2.22}$$

where J is the hopping parameter, Δ the strength of the on-site potential, β is the ratio between the frequencies of the two optical potentials generating the lattice, and ϕ is an arbitrary phase. The hopping parameter and the on-site potential can be derived from the local forces and potentials acting on the atoms. This model is commonly known as Aubry-André model, and for an irrational β, i.e. when the frequencies of the two optical potentials generating the lattice are incommensurate, the on-site potential is quasi-periodic [85–88]. The interest in this model, even in the non interacting case, is due to the fact that it allows us to explore localisation phenomena in a controllable and tunable way. Indeed, for $\Delta > 2J$ the model shows a transition from delocalized to localized single particle eigenstates. The existence of this well defined critical point clearly makes the Aubry-André model a more exploitable platform when compared to other localised models such as the Anderson insulator. Furthermore, for $\Delta < 2J$ not only the eigenstates are delocalised but also the spectrum is absolutely continuous.

For $\Delta > 2J$ the spectrum is known to be pure point and the eigenstates exponentially localised. Finally, for $\Delta = 2J$ the spectrum is singular continuous and the eigenstates are *critical* [89], i.e. they are characterised by a power-law decay of the amplitudes.

Chapter 3

Probing Protocols

The ultimate goal of a probing protocol is to learn about the properties and the characteristics of the system to which it is applied. When the target of such investigation is a quantum system one is generally interested in two characterizing quantities, namely, the density matrix and the Hamiltonian. The former one is the operator describing the quantum state of the system, may it be pure or mixed, and encodes information about coherences, correlations and the expectation values of any observable we can measure. The latter is the operator ruling the dynamics of the system. It determines its spectral properties, such as the eigenenergies, and its equilibrium properties, such as the ground state configuration. Studying the ground state of a system and its changes when varying a control parameter is the key to understand quantum phase transitions and other critical phenomena.

In what follows we review the results of papers I-III and VIII and employ the quantum probing paradigm in order to extract information about the state of the system, prior to the probing protocol, and the features determined by its Hamiltonian, such as the energy of its excitations and eventual criticality.

3.1   Momentum-Resolved Spectroscopy

Momentum-resolved-spectroscopy [90, 91] aims at measuring the dispersion relation $\omega(\mathbf{k})$ connecting frequency and momentum of the excitation modes of the system. When dealing with bosons/fermions in a lattice we need to impose translational symmetry in order to be able to define, according to Bloch theorem, the *crystal momentum*. Let us consider an environment

Hamiltonian

$$\hat{H}_E = \sum_{\mathbf{k}} \omega_{\mathbf{k}} \hat{b}_{\mathbf{k}}^{\dagger} \hat{b}_{\mathbf{k}}, \tag{3.1}$$

where $\omega_{\mathbf{k}}$ are the environment modes eigenfrequencies and $\hat{b}_{\mathbf{k}}^{\dagger}$ and $\hat{b}_{\mathbf{k}}$ are the related creation and annihilation operators. The index $\mathbf{k}$ in Eq. (3.1) identifies the momentum associated to the excitation of energy $\omega_{\mathbf{k}}$.

   We have designed a protocol to perform momentum-resolved spectroscopy using a single localised quantum probe relying on the following few assumptions:

(1) a complete knowledge of the probe, meaning that we need to know its Hamiltonian $\hat{H}_P = \sum_{\bar{n}} \epsilon_{\bar{n}} |\bar{n}\rangle\langle\bar{n}|$ and the related eigensystem $\{\epsilon_{\bar{n}}, \psi_{\bar{n}}(\mathbf{x})\}$;

(2) weak interaction between the environment and the probe;

(3) controllability of the probe via some external parameter;

(4) total system at the initial time in the factorised state $\hat{\rho}(t_0) = |\bar{g}\rangle\langle\bar{g}| \otimes \hat{\rho}_E$, where $|\bar{g}\rangle$ is a known state of the probe, possibly its ground state, and the environment is in a thermal state $\hat{\rho}_E = e^{-\beta\hat{H}_E}/\mathcal{Z}_E$.

Without loss of generality, we can take the following interaction Hamiltonian

$$g\hat{H}_{int} = g \sum_{\epsilon_{\bar{m}} > \epsilon_{\bar{n}}} |\bar{m}\rangle\langle\bar{n}| \otimes \hat{\Phi}[\bar{m},\bar{n}] + g \sum_{\epsilon_{\bar{m}} < \epsilon_{\bar{n}}} |\bar{m}\rangle\langle\bar{n}| \otimes \hat{\Phi}^{\dagger}[\bar{m},\bar{n}], \tag{3.2}$$

where $\hat{\Phi}[\bar{m},\bar{n}] \propto \sum_{\mathbf{k}} \gamma_{\bar{m},\bar{n}}^{\mathbf{k}} \hat{b}_{\mathbf{k}}$ ($\hat{\Phi}^{\dagger} \propto \sum_{\mathbf{k}} \gamma_{\bar{m},\bar{n}}^{\mathbf{k}} \hat{b}_{\mathbf{k}}^{\dagger}$) describes the absorption (emission) of environment excitations related to the probe transitions $|\bar{n}\rangle \to |\bar{m}\rangle$ and weighted by the amplitudes $\gamma_{\bar{m},\bar{n}}^{\mathbf{k}}$.

   The protocol consists in selecting two eigenstates of the probe, namely $|\bar{g}\rangle$ and $|\bar{e}\rangle$, whose transition frequency $\nu \equiv \epsilon_{\bar{e}} - \epsilon_{\bar{g}}$ is tunable trough an external parameter. Due to the weak coupling condition the total time-dependent transition probability from $|\bar{g}\rangle$ to $|\bar{e}\rangle$ obtained using Eq. (1.29) reads

$$\Gamma_{\bar{g}\to\bar{e}}(t) = g^2 \int_0^t dt_1 \int_0^t dt_2 \langle\hat{\Phi}^{\dagger}[\bar{g},\bar{e}](t_1)\hat{\Phi}[\bar{e},\bar{g}](t_2)\rangle e^{-i\nu(t_1-t_2)}. \tag{3.3}$$
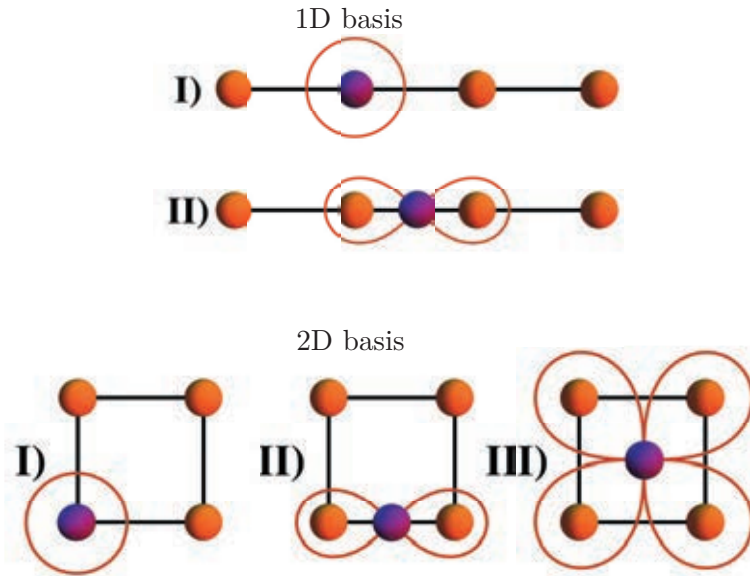
Figure 3.1: An example of a good configuration for the multistep measurements of the momentum-resolved spectroscopy protocol for a square lattice geometry in 1D and 2D. In the first measurement (I) the probe interacts only with one site. In the second one (II) it is interacting equally with two adjacent sites. In the third step (III), for the 2D geometry, the probe is equally coupled to all the four sites of the cell.

We now consider, for each mode $\omega_{\mathbf{k}}$ and related ladder operators $\hat{b}_{\mathbf{k}}$, the corresponding Bloch function $w_{\mathbf{k}}(\mathbf{x})$[1]. Furthermore, we assume the amplitudes $\gamma^{\mathbf{k}}_{\bar{m},\bar{n}}$ in Eq. (3.2) to be proportional to some overlap integrals, $\gamma^{\mathbf{k}}_{\bar{m},\bar{n}} = \int d\mathbf{x} \, \psi^*_{\bar{e}}(\mathbf{x})\psi_{\bar{g}}(\mathbf{x})w_{\mathbf{k}}(\mathbf{x})$. The Bloch functions can be expanded in terms of site-localised Wannier functions as $w_{\mathbf{k}}(\mathbf{x}) = \sum_{\mathbf{r}} \gamma_{\mathbf{k}} e^{i\mathbf{k}\mathbf{r}} W_{\mathbf{r}}(\mathbf{x})$. We can impose the probe to be local, i.e. its eigenfunctions to be localised on one lattice site, say $\mathbf{0}$, so that the only relevant overlap integral is the one involving the corresponding Wannier function, $W_{\mathbf{0}}(\mathbf{x})$.

The transition rate is then given by

$$\tilde{\Gamma}_{\bar{g}\to\bar{e}}(t) \equiv \Gamma_{\bar{g}\to\bar{e}}(t)/g^2 t^2 = \sum_{\mathbf{k}} |J_{\mathbf{0}}\gamma_{\mathbf{k}}|^2 \operatorname{sinc}^2\left[\frac{(\nu - \omega_{\mathbf{k}})t}{2}\right] n_{\mathbf{k}}, \qquad (3.4)$$

---

[1]We confine the dynamics to the lowest Bloch band.

where $J_0 = \int d\mathbf{x} \, \psi_{\bar{e}}^*(\mathbf{x}) \psi_{\bar{g}}(\mathbf{x}) W_0(\mathbf{x})$ and $n_\mathbf{k}$ is the average number of thermal excitations at frequency $\omega_\mathbf{k}$. When measuring the transition rate of Eq. (3.4) as a function of the probe frequency ν, one will observe resonance peaks revealing the excitation spectrum of the environment. The amplitudes of such peaks are given by $A_\mathbf{k}^2 = d_\mathbf{k} |J_0 \gamma_k|^2 n_\mathbf{k}$, where $d_\mathbf{k}$ is the $\mathbf{k}$-th mode degeneracy. In order to perform a full momentum-resolved spectroscopy more information is needed to reconstruct the full dispersion relation $\omega(\mathbf{k})$. In article II we have found that this can be achieved by measuring the transition probabilities while properly tailoring how and which Wannier states contributes to the overlap integral. More specifically, if the geometry of the lattice is known, the ratio between the amplitudes of the resonant peaks obtained from these extra measurements and those of the first one is found to satisfy a set of equations of the form

$$\frac{A_\mathbf{k}^{2\,i}}{A_\mathbf{k}^2} = \left| \frac{J_\mathbf{i}}{J_0} \right|^2 \sum_{\mathbf{k}|\nu=\omega_\mathbf{k}} G_i(\mathbf{k}), \quad i = 1, ..., d \tag{3.5}$$

where $J_\mathbf{i}$ are overlap integrals and $G_i(\mathbf{k})$ are functions of the momentum which depend on the specific geometry of the lattice. We have found that the number of extra measurements needed to perform momentum reconstruction is related to the dimensionality of the system to be probed; if d is the dimension of the lattice we need a total of $d + 1$ sets of measurements. For a 1D and a 2D square lattice the extra measurements need to be performed by a probe interacting equally with the neighbouring sites, as depicted in Fig. 3.1. These yield for the 1D lattice

$$\sum_{k|\nu=\omega_\mathbf{k}} G(k) = 4\cos^2\left(\frac{ka}{2}\right), \tag{3.6}$$

and for the 2D lattice

$$\sum_{\mathbf{k}|\nu=\omega_\mathbf{k}} G_i(\mathbf{k}) = \begin{cases} 2\cos^2\left(\frac{k_x a}{2}\right) + 2\cos^2\left(\frac{k_y a}{2}\right) & i = 1 \\ 16\cos^2\left(\frac{k_x a}{2}\right)\cos^2\left(\frac{k_y a}{2}\right) & i = 2 \end{cases}. \tag{3.7}$$

It is worth mentioning that, in order to observe the resonant peaks, the time of measurement should be larger then the typical time scale associated to the low-energy portion of the spectrum but short enough to guarantee the validity of the perturbative approach.

In what follows we apply the protocol to perform momentum-resolved spectroscopy to a 1D superfluid and to a 1D Kitaev chain with long range tunnelling.

3.1.1 Probing the spectrum of a superfluid

In a certain physical systems a step by step microscopic derivation of the assumptions made for the proposed protocol is possible. This is for instance the case of a system of condensed bosons in an optical lattice, i.e. the superfluid phase of a Bose-Hubbard system, explored in detail in Article VI. The probe can be modelled as an impurity atom interacting with the the Bose gas via a density-density interaction, with the usual assumption of a contact potential

$$g\hat{H}_{int} = g \sum_{\bar{n},\bar{m}} \int d\mathbf{x}\ \psi_{\bar{m}}^*(\mathbf{x})\psi_{\bar{n}}(\mathbf{x})|\bar{m}\rangle\langle\bar{n}| \otimes \hat{\Phi}^\dagger(\mathbf{x})\hat{\Phi}(\mathbf{x}), \qquad (3.8)$$

where $\hat{\Phi}(\mathbf{x})$ is the Bose gas field operator. The probe is taken to be an impurity in a 3D harmonic trap, whose frequencies in the three directions can be tuned independently. The unperturbed probe wave functions in (3.8) are then $\psi_{\bar{n}}(\mathbf{x}) = \psi_{n_x}^{(\nu_0)}(x)\psi_{n_y}^{(\nu_0)}(y)\psi_{n_z}^{(\nu)}(z)$. With this probe design we are interested in measuring transition probabilities between impurity states along the axis orthogonal to the lattice, say the z direction, and we assume the x and y degrees of freedom to be frozen. In this case ν is our controllable parameter and $\Gamma_{\bar{0}\to(0,0,n_z)}(\nu)$ is the transition rate, analogous to Eq. (3.3), which we want to measure in order to extract the Bogoliubov frequencies of the superfluid. For a 1D Bose-Hubbard model, with motion along the x axis, we can expand the field modes in Eq. (3.8) in terms of Wannier states [92] and get

$$g\hat{H}_{int} = g \sum_{n,m;i,j} \int dxdydz\ \psi_{\bar{n}}^*(x,y,z)\psi_{\bar{m}}(x,y,z)\times$$
$$W_i^*(x)W_j(x)\delta_i(y,z)\delta_j(y,z)|\bar{n}\rangle\langle\bar{m}| \otimes \hat{c}_i^\dagger\hat{c}_j, \qquad (3.9)$$

To compute the transition rates of Eq. (3.3) in the weak coupling regime $\langle 0, 0, n_z|\hat{H}_{int}|0, 0, 0\rangle$ is needed. For the first measurement the probe is cou-

pled only to one lattice site, say 0, leading to

$$\langle 0, 0, n_z | \hat{H}_{int} | 0, 0, 0 \rangle \simeq \psi_{n_y=0}(y=0)^2 \psi_{n_z=0}(z=0) \psi_{n_z}(z=0)$$
$$\times \int dx \, \psi_{n_x=0}(x)^2 W_0^2(x) \hat{c}_0^\dagger \hat{c}_0, \tag{3.10}$$

while for the second measurement the probe is coupled with equal strength to two adjacent sites, say 0 and 1, giving

$$\langle 0, 0, n_z | \hat{H}_{int} | 0, 0, 0 \rangle \simeq \psi_{n_y=0}(y=0)^2 \psi_{n_z=0}(z=0) \psi_{n_z}(z=0)$$
$$\times \int dx \, \psi_{n_x=0}(x - \frac{a}{2})^2 \sum_{i,j=0,1} W_i(x) W_j(x) \hat{c}_i^\dagger \hat{c}_j. \tag{3.11}$$

Expanding the bosonic operators in the Bogoliubov modes and retaining terms at most of order $\sqrt{N_0}$, i.e. the macroscopic condensate occupation, Eqs. (3.10)-(3.11) can be recast as follows

$$\langle 0, 0, n_z | \hat{H}_{int} | 0, 0, 0 \rangle_a \simeq \phi m (-1)^{n_z} \frac{\gamma_{n_z}^{1/2} \gamma_0^{3/2}}{\pi^2} \sqrt{\nu \nu_0} \times \tag{3.12}$$

$$\left[n_0 + \sqrt{n_0} \sum_{k \neq 0} \beta_k \left(e^{ikx_i} \hat{b}_k^\dagger + e^{-ikx_i} \hat{b}_k \right) \right], \quad \tag{3.13}$$

and

$$\langle 0, 0, n_z | \hat{H}_{int} | 0, 0, 0 \rangle_b \simeq (\varphi + \varphi') m (-1)^{n_z} \frac{\gamma_{n_z}^{1/2} \gamma_0^{3/2}}{\pi^2} \sqrt{\nu \nu_0} \times$$

$$\left\{ 2n_0 + \sqrt{n_0} \sum_{k \neq 0} \beta_k \left[\left(e^{ikx_1} + e^{ikx_0} \right) \hat{b}_k^\dagger + \text{h.c.} \right] \right\}, \tag{3.14}$$

in which we have introduced the Euler Gamma function ratio $\gamma_n = \frac{\Gamma(n+1/2)}{\Gamma(n+1)}$. The relevant overlap integrals appearing in Eqs. (3.13)-(3.14) are $\phi = \int dx \, \psi_{n_x=0}^2(x) W_0^2(x)$, $\varphi = \int dx \, \psi_{n_x=0}(x - a/2)^2 W_{0/1}^2(x)$, and $\varphi' = \int dx \, \psi_{n_x=0}(x - a/2)^2 W_{0/1}(x) W_{1/0}(x)$.

Measuring the transition rates in these two configurations and calculating the ratio of Eq. (3.5) naturally leads to a set of equation which satisfy
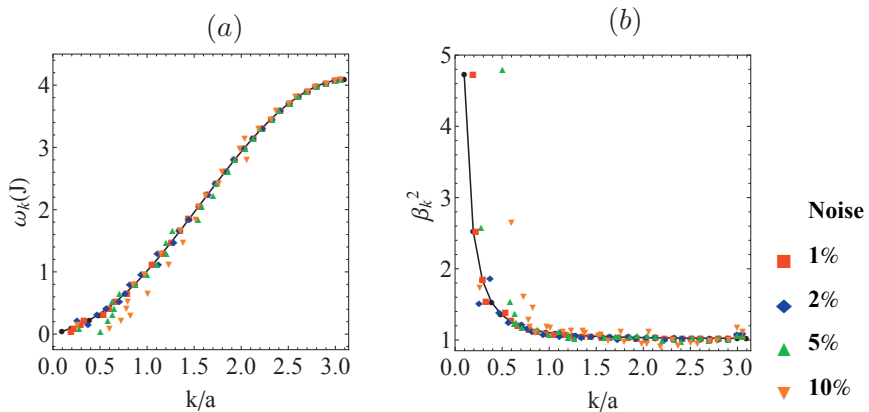
Figure 3.2: Comparison between the analytic excitation spectrum $\omega(k)/\beta_k^2$ (black dot) and the frequencies extracted via the probing protocol using the local atomic probe in (a) and (b) respectively. To the ratio of different resonant peaks has been applied a random noise of of 1% (red), 2% (blue), 5% (green) and 10% (orange).

the condition of Eq. (3.6). As an example we show the reconstructed dispersion relation in panel (a) of Fig. 3.2, and compare it with the exact analytic values $\omega(k)$. The reconstructed points in Fig. 3.2 take into account the presence of statistical noise. All the reconstructed curves are able to capture the relevant features and behaviour of the the Bogoliubov spectrum. One can also extract the spectral density β_k from the amplitude of the resonant peaks. Panel (b) of Fig. 3.2 shows the comparison between the exact spectral density and the reconstructed ones for the same sources of error considered for the spectrum, and again the main features are well captured. It is worth noticing that because of the specific form of the equation to solve, (3.6), the quantities at low k are more sensitive to noise.

3.1.2 Probing the spectrum of a 1D Kitaev chain

We now apply the proposed momentum-resolved spectroscopy protocol to the Kitaev chain of Eq. (2.17). For simplicity we assume the probe to be a two-level system and that the two following interaction Hamiltonians,
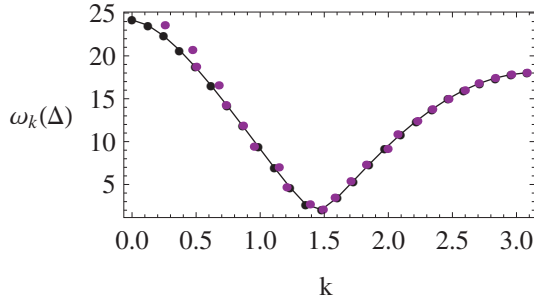
Figure 3.3: Single-particle spectrum of the Kitaev chain. The black dots are the exact values, while the purple dots are those reconstructed via the momentum-resolved spectroscopy protocol.

necessary for the two-step protocol, can be efficiently engineered

$$\hat{H}_{int}^{I} = g \sum_k \left\{ \hat{\sigma}^+ \cos(\theta_k/2)\hat{c}_k + \hat{\sigma}^- \cos(\theta_k/2)\hat{c}_k^\dagger \right\}, \tag{3.15}$$

$$\hat{H}_{int}^{II} = g \sum_k \left\{ \hat{\sigma}^+ [1 + \cos(k)] \cos(\theta_k/2)\hat{c}_k + \hat{\sigma}^- [1 + \cos(k)] \cos(\theta_k/2)\hat{c}_k^\dagger \right\}. \tag{3.16}$$

The above interaction Hamiltonians have precisely the form given in Eq. (3.2), with $\hat{\Phi}^{\text{I}}[\bar{e}, \bar{g}] = \sum_k \cos(\theta_k/2)\hat{c}_k$ and $\hat{\Phi}^{\text{II}}[\bar{e}, \bar{g}] = \sum_k [1+\cos(k)] \cos(\frac{\theta_k}{2})\hat{c}_k$ in the two cases. Our aim here is to show the feasibility of the protocol for probing fermionic systems showing that it is possible to reconstruct also non-monotonic spectra. Fig. 3.3 displays the reconstructed spectrum, which even in the presence of noise, shows a good agreement with the exact values.

3.2 A single qubit thermometer

In several physical contexts, experiments on quantum systems are carried out at very low temperatures, being them cold atomic gases or superconducting systems. Generally, low temperatures allow us, e.g., to prolong coherence times, to explore low energy physics, Bose-Einstein condensation, superfluidity and superconductivity. Therefore, it is crucial to develop a

reliable quantum thermometer in such an extreme temperature regime. In this framework the possibility of using a quantum probe to realise a single qubit thermometer has been extensively explored [93–97]. We proposed and tested a scheme to perform thermometry on a Bose gas trapped in an optical lattice based on the immersion of a quantum probe whose coupling is controlled in a non-adiabatic way. The temperature of the gas is estimated via Crooks-Tasaki fluctuation relations, once the work distributions are extracted trough the related characteristic functions [2] [12, 98].

We label the levels of the qubit-thermometer with $|\downarrow\rangle$ and $|\uparrow\rangle$ and we take the time-dependent interaction Hamiltonian to be of the form

$$\hat{H}_{int}(t) = (g_\downarrow(t)|\downarrow\rangle\langle\downarrow| + g_\uparrow(t)|\uparrow\rangle\langle\uparrow|) \otimes \hat{V}. \tag{3.17}$$

The total system at the inital time $t = 0$ is prepared in the state $\hat{\rho} = |s\rangle\langle s| \otimes \hat{\rho}_E(\beta)$, with the qubit in some superposition $|s\rangle = s_\downarrow|\downarrow\rangle + s_\uparrow|\uparrow\rangle$ and the environment obviously in a thermal state. Crucial to the thermometric protocol is the control over the state-dependent couplings $g_\downarrow(t)$ and $g_\uparrow(t)$, which need both to be varied as follows

$$g_\downarrow(t) = \begin{cases} g(t), & 0 \leq t \leq \tau, \\ g(\tau), & \tau \leq t \leq \tau + u, \end{cases}$$

$$g_\uparrow(t) = \begin{cases} g(0), & 0 \leq t \leq u, \\ g(t-u), & u \leq t \leq \tau + u. \end{cases}$$

The function $g(t)$ describes the quench protocol for the two couplings, which have the same temporal profile but with a delay. At time $\tau + u$, when both quenches are complete, the qubit-thermometer is in the reduced state

$$\begin{aligned} \hat{\rho}_q =& |s_\downarrow|^2|\downarrow\rangle\langle\downarrow| + s_\uparrow^* s_\downarrow e^{i\Delta(\tau+u)}\chi^*(u)|\downarrow\rangle\langle\uparrow| \\ &+ s_\downarrow^* s_\uparrow e^{-i\Delta(\tau+u)}\chi(u)|\uparrow\rangle\langle\downarrow| + |s_\uparrow|^2|\uparrow\rangle\langle\uparrow|. \end{aligned} \tag{3.18}$$

where $\chi(u)$ is the dephasing function

$$\chi(u) = \mathrm{Tr}\left\{\hat{U}_Q^\dagger e^{iu\hat{H}(g(\tau))}\hat{U}_Q e^{-iu\hat{H}(g(0))}\hat{\rho}_E\right\}. \tag{3.19}$$

---

[2]The idea of applying the Crooks-Tasaki relations for inferring the temperature of a quantum system has a wide range of applicability and it is basically system-independent.
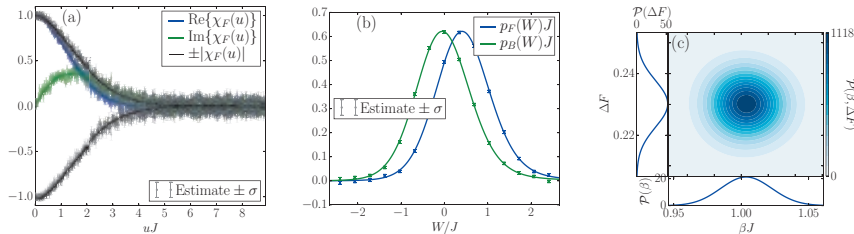
Figure 3.4: (a) Characteristic function $\chi_F(u)$ of the forward quench. (b) Work distributions $P_F(W)$. (c) The joint distribution $\mathcal{P}(\beta, \Delta F)$, together with the corresponding marginal distributions $\mathcal{P}(\beta)$ and $\mathcal{P}(\Delta F)$.

$\hat{U}_Q = \mathcal{T} \exp[-\mathrm{i} \int_0^\tau \mathrm{d}t \hat{H}(g(t))]$ is the time evolution operator that evolves the system according to the time-dependent quench Hamiltonian. As a consequence of the specific protocol (3.18), $\chi(u)$ corresponds to the characteristic function, or Fourier transform, of the forward work distribution. By inverting (3.18), one can obtain also the backward work distribution and then infer the temperature via the Crooks-Tasaki relation

$$\ln\{R(W)\} = \ln\left\{\frac{P_F(W)}{P_B(-W)}\right\} = \beta(W - \Delta F). \tag{3.20}$$

One way of extracting the characteristic function $\chi(u)$ is by measuring the expectation values of $\hat{\sigma}_x$ and $\hat{\sigma}_y$, since they are related by the simple relation

$$\langle \hat{\sigma}_x \rangle + \mathrm{i}\langle \hat{\sigma}_y \rangle = 2s_\downarrow^* s_\uparrow \mathrm{e}^{-\mathrm{i}\Delta(\tau+u)} \chi(u). \tag{3.21}$$

Fig. 3.4 summarises some of the finding of paper I and shows, as an example, the characteristic function of the forward protocol (a), the forward and backward work distribution (b), and the estimation of the temperature of the system and the free energy difference (c). The results are shown for the case of a finite temperature superfluid taking into account the error deriving from a finite number of measurements.

3.3   Probing criticality

Besides having fundamental importance when studying the irreversibility of a quantum quench, the irreversible work is a powerful tool to explore crit-

ical phenomena and quantum phase transitions [99–104]. Quantum phase transitions are usually characterised by an abrupt change of the ground state properties as the parameter driving the phase transition is varied through the critical point. In this perspective, the usefulness of the irreversible work becomes clear and straightforward, once the link with the ground state energy is established.

Following [100] let's take an Hamiltonian of the form

$$\hat{H}(\epsilon) = \hat{H}_0 + \epsilon\hat{V}, \tag{3.22}$$

and consider a quench in ϵ, from an initial value ϵ_i to a final one ϵ_f. The average work done during an infinitesimal quench at zero temperature is

$$\langle W \rangle = \langle \hat{H}(\epsilon_f) - \hat{H}(\epsilon_i) \rangle \simeq \delta\epsilon \frac{\partial E_{GS}(\epsilon)}{\partial \epsilon}\bigg|_{\epsilon_i}, \tag{3.23}$$

where $\delta\epsilon = \epsilon_f - \epsilon_i$. To derive Eq. (3.23) one has to use $\hat{V} = \partial\hat{H}(\epsilon)/\partial\epsilon$ and the Hellmann-Feynman theorem [105]. Consequently, the irreversible work produced during the quench, obtained by subtracting the free energy difference to the average work, can be written as

$$W_{irr} = \delta\epsilon \frac{\partial E_{GS}(\epsilon)}{\partial \epsilon}\bigg|_{\epsilon_i} - E_{GS}(\epsilon_i) + E_{GS}(\epsilon_f) \simeq -\frac{\delta\epsilon^2}{2}\frac{\partial^2 E_{GS}(\epsilon)}{\partial \epsilon^2}\bigg|_{\epsilon_i}. \tag{3.24}$$

We now can see from Eq. (3.24) the link between the second derivatives of the ground state energy and the irreversible work production of infinitesimal quantum quenches.

At finite temperature, considering the system in an initial thermal state at inverse temperature β, a similar relation holds. In this case, for an infinitesimal quench, the irreversible work is proportional to the second derivative of the equilibrium free energy $F_\beta(\epsilon)$:

$$W_{irr} \simeq -\frac{\delta\epsilon^2}{2}\frac{\partial^2 F_\beta(\epsilon)}{\partial \epsilon^2}\bigg|_{\epsilon_i}. \tag{3.25}$$

Eq. (3.25) establishes a connection between the irreversible work and the specific heat $C \propto -\frac{\partial^2 F_\beta(\epsilon)}{\partial \epsilon^2}$ [56].

3.3.1 Coulomb Crystals: linear to zig-zag transition

We now focus on the non-equilibrium statistics of the irreversible work produced during sudden and infinitesimal quenches in proximity of the structural linear-zigzag transition in ion Coulomb crystals. We quench the transverse trapping frequency ω in Eq. (2.15) from $\omega_i = \omega$ to ω_f, such that $|\omega_i^2 - \omega_f^2| = \Delta\omega$. For a quench within the same phase, in the harmonic approximation, analytical calculations can be made and we find the following analytical expressions for the irreversible work W_{irr} and the statistical variance σ_W^2

$$W_{irr} = \sum_k \left[\frac{1}{2} \left(\Omega_k \omega_k^f - \omega_k^i \right) \coth \frac{\beta\omega_k^i}{2} - \frac{1}{\beta} \ln \frac{\sinh\left(\frac{\beta\omega_k^f}{2}\right)}{\sinh\left(\frac{\beta\omega_k^i}{2}\right)} \right], \qquad (3.26)$$

and

$$\sigma_W^2 = \sum_k \frac{\omega_k^{f\,2} \cosh(\beta\omega_k^i)\left(\Omega_k^2 - 1\right) + \left(\omega_k^f \Omega_k^2 - \omega_k^i\right)^2}{4\sinh^2(\beta\omega_k^i/2)}, \qquad (3.27)$$

where $\omega_k^{i/f}$ is the initial/final frequency of the $k-$mode and $\Omega_k = \frac{\omega_k^{i2} + \omega_k^{f2}}{2\omega_k^i \omega_k^f}$. The range of validity of such formulas is actually quite wide and, in fact, they turn out to hold for any quench that does not alter the symmetries of the system.

On both the linear and the zig-zag sides of the transition, the irreversible work as well as the statistical variance are monotonically increasing functions of ω^2, when approaching the critical point h_1, as displayed in Fig. 3.5, and they behave like extensive quantities. It is interesting to isolate the contribution of the soft mode to the irreversible work and to the variance, since the soft mode is responsible of the vanishing gap at the critical point. Limiting then the sums in Eqs. (3.26)-(3.27) to $k = \pi$ and expanding up to second order in $\Delta\omega^2$ we obtain

$$W_{irr}^{\text{soft}} = \frac{g\Delta\omega^2}{8\gamma_W |\omega^2 - h_1|^{3/2}} + \mathcal{O}(\Delta\omega^3), \qquad (3.28)$$

$$\sigma_{\text{soft}}^2 = \frac{g^2\Delta\omega^2}{\gamma_\sigma |\omega^2 - h_1|} + \mathcal{O}(\Delta\omega^3). \qquad (3.29)$$

Both expressions are valid in the linear phase for $\gamma_W = 2$ and $\gamma_\sigma = 8$ and in the zigzag phase for $\gamma_W = \sqrt{2}$ and $\gamma_\sigma = 4$. It is worth noticing that Eq. (3.29) for σ_{soft}^2 is exact in the linear phase. The soft mode contributions are summarised in panels (c) and (d) of Fig. 3.5. When all the other
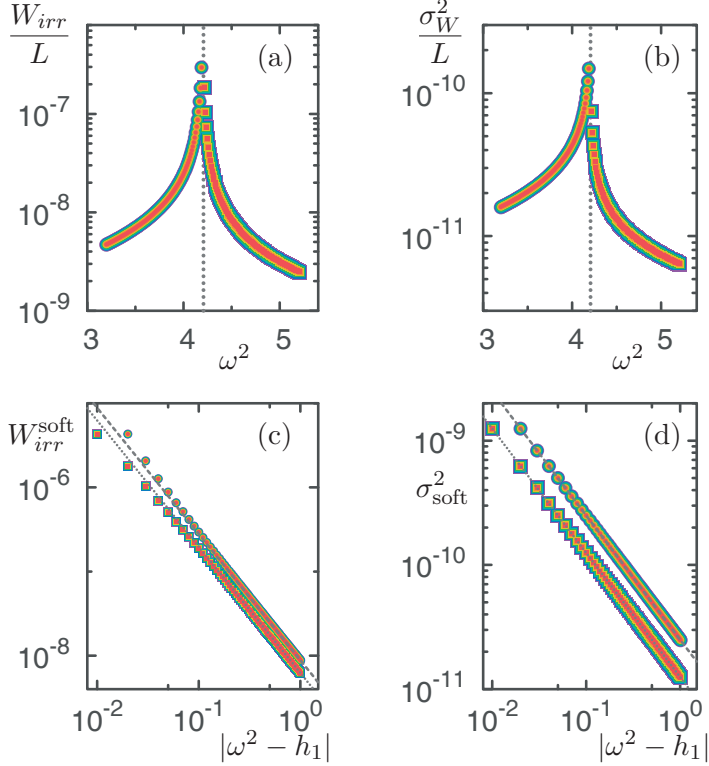

Figure 3.5: Upper panels: Irreversible work W_{irr} (a) and the variance σ_W^2 (b) for small quenches with amplitude $\Delta\omega = 0.01$ within the same phase at zero temperature as a function of the initial frequency squared ω^2. The vertical dotted line indicates the critical frequency. Lower panels: Contribution of the soft mode to the irreversible work W_{irr} (c) and the variance σ^2 (d) as a function of $|\omega^2 - h_1|$. The straight lines are the approximate scaling expressions. The chain sizes consiered are $L = 60$, 72, 90, 108, 120, 132, and 144 in purple, blue, cyan, green, yellow, orange and red, respectively. Squares and circles are used for the linear and zig-zag phase, respectively.

modes are taken into account the typical scaling is modified and in the

thermodynamic limit, close to criticality, we can expand Eq. (3.26). In the linear phase we find

$$
\begin{aligned}
W_{irr} &= \sum_k \frac{(\omega_k^f - \omega_k^i)^2}{4\omega_k^i} \simeq L \int dk \, \frac{(\omega_k^f - \omega_k^i)^2}{4\omega_k^i} \\
&\sim L \log\left(\omega^2 - h_1\right) + A,
\end{aligned} \tag{3.30}
$$

and a similar expression holds also in the zig-zag phase.

The irreversible work (3.26) might be a difficult quantity to measure in an experimental setup. However, for the quench considered, the average work is

$$
\langle W \rangle = \langle \Psi_G(\omega_i)| \left[H(\omega_f) - H(\omega_i) \right] |\Psi_G(\omega_i)\rangle = \frac{1}{2} \Delta\omega \mathcal{Y}^2(\omega), \tag{3.31}
$$

where $\mathcal{Y}^2(\omega) = \sum_j \langle \Psi_G(\omega)|y_j^2|\Psi_G(\omega)\rangle$ represents the total fluctuation of the transverse displacement operators. Measuring this quantity is in the grasp of the experimentalists in trapped-ion setups [106–109]. Therefore, for an infinitesimal quench, thanks to Eq. (3.24), the irreversible work can be obtained by taking the derivative of Eq. (3.31).

3.4   Chapter summary and discussion

In this Chapter we have presented the results of Publications I, II, III and VIII. These works follow a different approach to quantum probing: I, II and VIII rely on engineering a controllable impurity, while III rely on the control of an external field driving a phase transition.

The main advantages of the former approach consist in the fact that the measurements are performed exclusively on the probe and that, within the limit of the assumptions made to design the probing protocol, the procedures outlined are basically platform independent. The momentum-resolved-spectroscopy protocol and the single qubit thermometry can be generally applied to a vast range of platforms, although we aimed at proving the feasibility of such procedures for a system of cold atoms trapped in optical lattices. Therefore, great attention was given into probing the Bose-Hubbard lattice in the superfluid regime. The disadvantages of these procedures are the high level of controllability required on the probe and the unavoidable consequence that the interaction with the probe, even in

the weak coupling regime, will bring the environment inevitably out of equilibrium.

The main advantages of the approach employed in Publication III are the high level of controllability already achieved and proved experimentally in tuning the frequencies of the anisotropic trap and the fact that the measurement are to be performed on equilibrium configurations. The downsides of this study are the absence of an actual, or rather external, read-out device and the fact that these findings are strictly related to the platform under investigation. In the particular case considered, linear to zig-zag structural phase transition of the Ion Coulomb Crystals, the criticality is explored trough measurements of the displacements of the ions composing the system and the quenched parameter is the frequency of the trap in the transverse direction. The procedure can be in principle extended to study in a similar fashion other phase transitions, when quenching the parameter driving the critical phenomenon, but then the measurements to perform may be not easily achieved experimentally as in this case.

Chapter 4

Memory Effects and Localisation

In this Chapter we present results, summarised in Publications IV and VI, focused on the connection between the probe Markovian or non-Markovian dynamical character and the quantum phase of the environment, to which the probe is coupled, exhibiting a quantum phase transition.

The idea of using the dynamics of an open system, and the possible presence of memory effects, to investigate quantum phase transitions is not new. In the past few years this approach has been employed to study, e.g., the transverse Ising model [24] and a system of trapped repulsively interacting ions known as Coulomb Crystals [25]. In the first case it was found that the paramagnetic and ferromagnetic phases both induce in the coupled probe a dynamics displaying memory effects, with the information backflow highly sensitive to the critical point. At the critical point, on the contrary, no information backflow is present and the probe dynamics is Markovian. In the second scenario, there exist two time regimes, corresponding to the cases in which the critical point displays a minimum or a maximum for the information backflow.

More recently, an array of coupled optical cavities with random disorder was investigated in Ref. [21], and it it is shown that non-Markovianity, quantified by a geometric measure [42], increases monotonically with the strength of the disorder. The dynamics in this case is always non-Markovian, and the source of memory effects is connected with Anderson localisation.

Motivated by these findings we have pushed forward the study of the possible link between localisation and the rise of memory effects, and the use of information backflow as a tool to witness quantum phase transitions.

We have focused on the superfluid-to-Mott insulator transition of the Bose-Hubbard model, that can be interpreted as a localisation phenomena induced by interaction. In this case, the repulsion between the bosons keep the particles localised. Then, we have studied the metal-to-insulator transition of a fermionic Aubry-André model. In this case the interplay between the tunnelling between neighbouring sites and the on-site quasi-periodic potential determines whether or not the single particle eigenstates are localised. This second model and its localisation phenomenology, induced by the potential, is somehow analogous to the Anderson localisation.

For these purposes, we have investigated the open dynamics of a quantum probe interacting with the Bose-Hubbard system or Aubry-André system trough an experimentally realisable interaction of the form

$$\hat{H}_{int} = U_e|e\rangle\langle e| \otimes \hat{n}_0. \tag{4.1}$$

Where we have taken the probe to be an effective two level system, characterised by the levels $|g/e\rangle$, and assumed that only one of its levels interacts with the lattice environment. The probe is then coupled to the local number operator $\hat{n}_0$, and can be seen as an impurity embedded in the lattice at site labelled as 0. U_e plays the role of an effective coupling constant that is assumed to be small in order to treat the probe as a small of perturbation [110].

According to Eq. (1.21) this interaction Hamiltonian leads to a purely dephasing dynamics for the probe, with the decoherence factor given by Eq. (1.22). By choosing the initial environment state to be a pure state $\hat{\rho}_E(t_0) = |\Phi\rangle\langle\Phi|$ the decoherence function can be written as

$$\chi(t) = \langle\Phi|e^{-i\hat{H}_e t}e^{i\hat{H}_g t}|\Phi\rangle, \tag{4.2}$$

where we have taken $t_0 = 0$ and $\hat{H}_{g/e} = \langle g/e|\hat{H}|g/e\rangle$. It is straightforward to see how (4.2) is related to the Loschmidt echo of the environment

$$L(t) = |\chi(t)|^2, \tag{4.3}$$

which represents the overlap between to states obtained by evolving the same initial state trough two different Hamiltonians. Qualitatively speaking, from the point of view of the environment, (4.3) is a measure of how different is the evolution in the presence of the probe when compared with

the free evolution. Furthermore, when $|\Phi\rangle$ is taken as an eigenstate of the environmental Hamiltonian without the probe, then $e^{i\hat{H}_g t}$ in (4.2) will result in a phase factor completely irrelevant when calculating (4.3). In this case the Loschmidt echo measures directly the dynamical deviation from the initial state due to the coupling with the probe.

4.1 Bose-Hubbard: Superfluid-to-Mott insulator transition

The Bose-Hubbard model (2.1) describes a systems of cold bosons trapped in an optical lattice. In general the model is analytically intractable. However, approximate models can be employed in specific cases . We have shown how the superfluid phase, $J \gg U$, can be described in terms of phonon-like excitations above the condensate fraction, (2.3), and the insulating phase, $U \gg J$, on the other hand can be described by fermionic quasi-excitations dubbed as doublons and holons, (2.12).

Therefore, in the two limiting cases the interaction (4.1) can be expanded in terms of the typical excitations characterising the Bose gas in the two phases. In the the superfluid regime the local number operator can be written as a the macroscopic condensate density n_0 plus a linear fluctuation in the Bogoliubov modes

$$\hat{H}_{int}^{SF} = U_e |e\rangle\langle e| \otimes \left[n_0 + \sum_k \frac{\beta_k}{N_S} \left(\hat{b}_k^\dagger + \hat{b}_k \right) \right], \qquad (4.4)$$

in which β_k is spectral density. In the the Mott insulator, according to the doublon-holon description, the local number operator can be first written as $\hat{n}_0 = \bar{n} + n_+ - n_-$, i.e. as the filling factor plus the difference between double occupancies and vacancies, and in terms of the normal modes the interaction Hamiltonian reads as

$$\begin{aligned} \hat{H}_{int}^{MI} = U_e |e\rangle\langle e| \otimes \Bigg[&\sum_{k,q} \cos\left(\frac{\theta_k - \theta_q}{2}\right) (\hat{d}_k^\dagger \hat{d}_q - \hat{h}_k^\dagger \hat{h}_q) \\ &+ i \sin\left(\frac{\theta_k - \theta_q}{2}\right) \left(\hat{d}_k^\dagger \hat{h}_{-q}^\dagger - \hat{h}_{-q} \hat{d}_k \right) + \bar{n} \Bigg], \end{aligned} \qquad (4.5)$$

where θ_k are the Bogoliubov angles appearing in the transformations of

Eq. (2.12). By fixing the environmental state $|\Phi\rangle$ to be the ground state, i.e. a vacuum of the normal excitations, we can compute, within these approximate models, the dephasing rates as in (1.20). For the superfluid we found

$$\gamma_{SF}(t) = U_e^2 \sum_k |\beta_k|^2 \frac{\sin(\omega_k t)}{N_s^2 \omega_k}, \tag{4.6}$$

and for the Mott insulator

$$\gamma_M(t) = U_e^2 \sum_{k,q} \sin^2\left(\frac{\theta_k - \theta_q}{2}\right) \frac{\sin(\omega_k^d + \omega_q^h)t}{N_s^2(\omega_k^d + \omega_q^h)}. \tag{4.7}$$

The two dephasing rates (4.6) and (4.7) share the same functional form, but they results in very different dynamics for the decoherence of the probe. Indeed, when embedding the impurity in the lattice it is not surprising to find that the Bose gas reacts differently in the two phases. For the non-Markovianity quantifier introduced in Eq. (1.24) memory effects occur clearly when the Loschmidt echo does not decay monotonically, but there are intervals of time in which it increases. This occurs whenever the dephasing rate appearing the master equation takes temporarily negative values.

In the superfluid regime, $L(t)$ displays revivals at long times only, due to finite size effects, see panel (a) of Fig. 4.1. The memory-inducing mechanism, in this case, is the following: after the impurity is embedded in the Bose lattice at site 0, representing the centre of the lattice, the repulsion generates a small depletion of the quenched site, and a fraction of the initial particles moves towards the neighbouring sites. A density wave is in this way generated, which travels freely throughout the lattice due to the superfluid regime. Revivals in the density of the quenched site (and, as a consequence, in the Loschmidt echo) are due to this wave reaching the boundary - because of the finite size - and bouncing back towards its source or simply coming back to the source in case of periodic boundaries. The revival time can be then estimated as N_s/c_s, where $c_s = \sqrt{2JUn_0}$ is the sound speed obtained from the phononic spectrum ans N_s is the number of lattice sites.

In the Mott insulator phase, the decoherence function shows the first revival at $\tau \simeq \frac{2\pi}{U}$, see panel ($b$) of Fig. 4.2. The Loschmidt echo reflects in
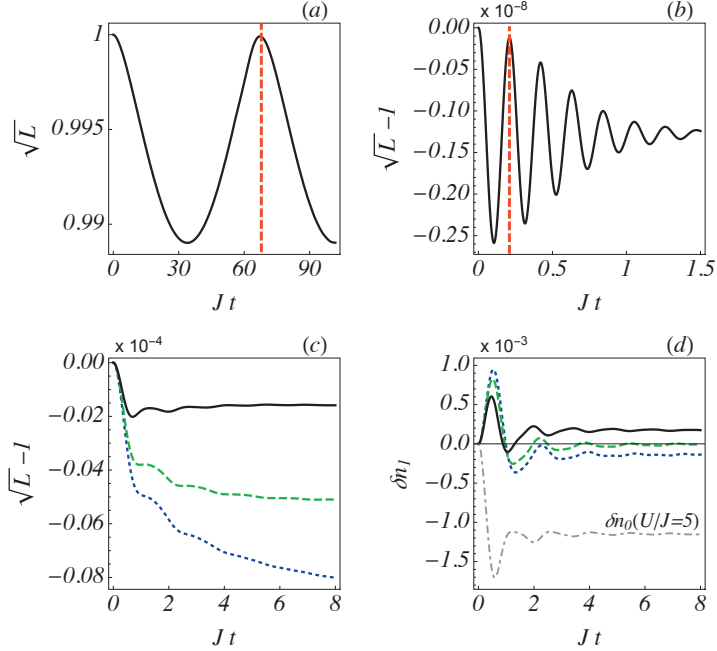
Figure 4.1: (a): Loschmidt echo in the superfluid phase calculated using Eq. (4.6) at $U/J = 1$, the vertical line is the recurrence time $\tau = \frac{N_S}{c_s} \simeq \frac{2\pi}{\omega_{k=2\pi/N_s}}$. ($b$): Loschmidt echo deep in the insulating phase at $U/J = 30$, the vertical line is $\tau = \frac{2\pi}{U}$. (c): Loschmidt echo in the intermediate regime for $U/J = 3.5, 4, 5$ in dotted blue, dashed green an solid black, respectively. (d): density fluctuations in the nearest neighbor of the pertubed site (dubbed as 1) for $U/J = 3.5, 4, 5$ in dotted blue, dashed green an solid black, respectively. The dot-dashed gray line gives the density fluctuation in the perturbed site for $U/J = 5$. In all the panels $U_e/J = 0.01$ and $N_s = 96$. Data displayed in (b), (c) and (d) were obtained trough particle-conserving ($\bar{n} = 1$) t-DMRG calculations.

this case the gap opened in the supefluid to Mott insulator transition, which is of order U. This revival time can be derived trough the doublons/holons description by noticing that, in the regime of strong interactions, the spectral density exhibits a maximum at $k = -q$ and $|k| \simeq \frac{\pi}{2}$. The energy of this doublon/holon pair is $2\Omega(\pi/2) \simeq U$, which is consistent with the revival
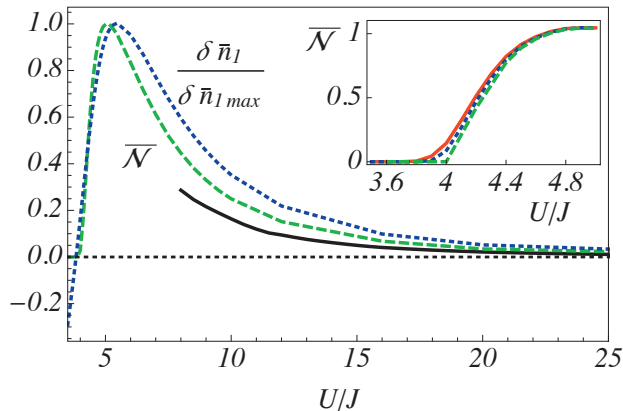
Figure 4.2: Comparison between numerical (dashed green, $N_s = 96$) and analytical (solid black, $N_S \to \infty$) normalised non-Markovianity measure $\overline{\mathcal{N}} = \mathcal{N}/\mathcal{N}_{\mathrm{max}}$ and average excess particle number at site 1, $\delta\bar{n}_1/\delta\bar{n}_{1\mathrm{max}}$ (dotted blue, $N_s = 96$), where the time average is performed over $JT = 2\pi$. In the inset, $\overline{\mathcal{N}}$ for different lattice sizes, $N_s = 80$, 96 and 128 in solid red, dotted blue and dashed green respectively.

time $\tau \simeq \frac{2\pi}{2\Omega(\pi/2)} = \frac{2\pi}{U}$. As a consequence the non-monotonicity of the Loschmidt echo occurs for shorter and shorter times for increasing values of the increasing interaction strength.

Fig. 4.2 displays the information backflow renormalised by its maximum value, i.e $\overline{\mathcal{N}} = \mathcal{N}/\mathcal{N}_{max}$, and summarises the aforementioned findings. It shows that the two limiting phases of the lattice gas are characterised by qualitatively different dynamics: fully Markovian when the environment is in the superfluid phase [1] and non-Markovian when the environment is deep in the Mott insulator phase. Between these two extreme analytical approaches are not available and one has to recur to fully numerical approaches. t-DMRG calculations[2] give evidence that the he Markovian-to-non-Markovian transition occurs at $(U/J)_{\mathcal{N}} \simeq 4$, different from, but still quite close to,s the critical point.

---

[1]The final time used to calculate the information backflow is truncated in order to exclude contributions due to finite size effects.

[2]Juan José Mendoza-Arenas is acknowledged for performing such t-DMRG simulations.

The onset of non-Markovian dynamics is then compared with the time averaged occupancy fluctuation of the impurity's adjacent site, labelled as site 1, $\delta \bar{n}_1 = 1/T \int_0^T \langle \hat{n}_1(t) \rangle - \langle \hat{n}_1 \rangle_{\mathrm{GS}}$. We notice how this quantity is negative for $U/J \lesssim 4$ and positive for greater values of U/J. Qualitatively speaking we see that the dynamics of the impurity is Markovian, even after the superfluid-to-Mott insulator critical point, the gas still maintains a certain level of mobility with a time-averaged density depletion on the neighbouring site. At larger interactions, particles accumulate (on average) and are trapped on site 1 and in this regime a signature of non-Markovian dynamics is witnessed.

The intuition is that the quasi-particles act as the physical information carriers and their dynamics is then connected to information backflow and non-Markovian memory effects. In the superfluid phase the density excitations travel freely in the gas and in the early Mott insulator phase, for $3.4 \lesssim U/J \lesssim 4$, higher occupancies are still able to propagate. The rise of memory effects is witnessed only when higher occupancies are instead trapped in the vicinity of the impurity.

To summarise, in Pubblication IV we have found that the information backflow experienced by the probe is able to distinguish the two regimes of the Bose-Hubbard model with a Markovian to non-Markovian crossover. Despite the fact that the crossover does not coincide with the critical point of the phase transition these findings strengthen the link between memory effects and localisation.

4.2 Aubry-André Model: metal-to-insulator transition

The fermionic version of the Aubry-André model (2.22) describes a systems of fermions trapped in a quasi-periodic geometry[3]. This setup is realisable in the field of cold atoms by means of a bichromatic optical lattice with incommensurate frequencies [82–84]. Even in the case of non-interacting particles, this model bears a rather rich physics. In a nutshell, for $\Delta/J < 2$ the single particles eigenstates are delocalized while for $\Delta/J > 2$ they are exponentially localised. This peculiar behaviour is often referred in literature as a metal-to-insulator transition.

---

[3]We always take β to be the golden ratio, i.e. $\beta = \frac{1+\sqrt{5}}{2}$.

In the following we consider, as initial state of the Fermi gas, a product state in the occupation basis, i.e., the so-called *charge density wave state*, in which only odd sites are initially occupied

$$|\Phi\rangle = \prod_{i\,\text{odd}} \hat{a}_i^\dagger |0\rangle, \tag{4.8}$$

where $|0\rangle$ represents the vacuum state. This state is particularly easy to realize in experiments and it has been previously used to explore relaxation properties [83], many-body localisation phenomena [84] and the decay of the Loschmidt echo in the presence of an impurity such as in (4.1), [111]. This choice for the initial state of the environment is peculiar in what it is not consistent with some of the assumptions generally made when performing a microscopic derivation of the master equation of the open system. Equation (4.8) indeed, is not an eigenstate of the unperturbed Hamiltonian and the environment will evolve in time even without the impurity. Therefore, we recurred to a fully numerical approach and computed the decoherence function, and in turn the Loschmidt echo, trough a determinant formula known as Levitov formula [112, 113]

$$\sqrt{L(t)} = |\chi(t)| = |\det(1 - \hat{n}_{cdw} + \hat{n}_{cdw} e^{-i\hat{h}_e t} e^{i\hat{h}_g t})|, \tag{4.9}$$

where $\hat{n}_{cdw} = \sum_{i\,\text{odd}} |i\rangle\langle i|$.

The two phases of the Aubry-André model give rise to very different behaviour of the Loschmidt echo as a function of the quasi-periodic potential and lattice size. In the delocalised phase the Loschmidt echo appears to decay in time without displaying any appreciable structure in the time scale considered. In this regime the decay gets faster and faster as the ratio Δ/J is increased. When increasing the lattice size, instead, the Loschmidt echo decays on longer time scales. These findings are displayed in panels (a) and (c) of Fig. 4.3. The localised regime shows instead a completely different behaviour. The decay of the Loschmidt echo is in fact suppressed by stronger values of the quasi-periodic potential and, as expected by a localised system, it is size independent. Furthermore, the decoherence factor is characterised by strong oscillations that, according to the Breuer-Piilo-Laine non-Markovianity measure are signal of information backflow and memory effects. These findings are displayed in (b) and (d) of Fig. 4.3. Panel (a) of Fig. 4.4 summarises these results in term of $\mathcal{R}$,
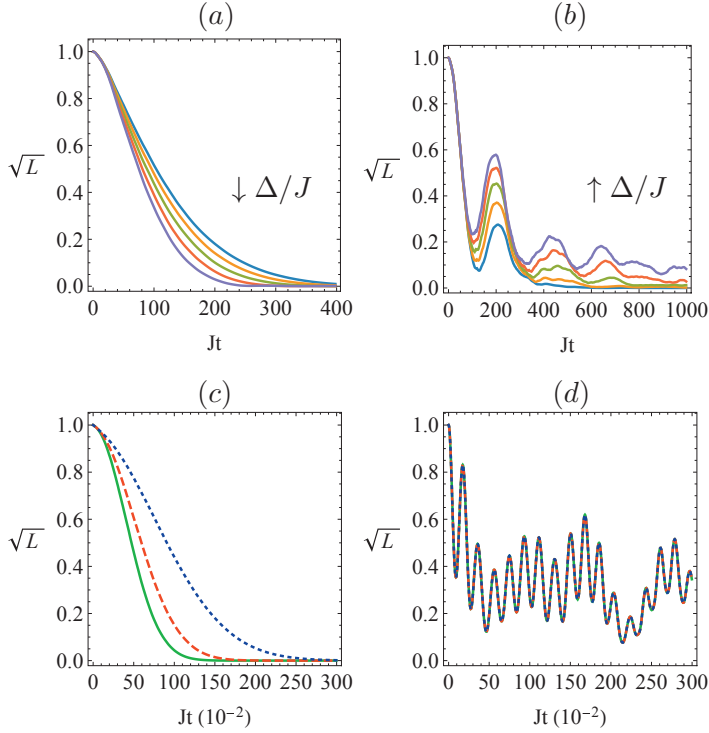
Figure 4.3: Square root of the Loshmidt echo. (a): $\sqrt{L(t)}$ for increasing Δ/J from blue to purple $(1.5 - 1.7)$. (b): $\sqrt{L(t)}$ for increasing Δ/J from blue to purple $(2.03 - 2.23)$. In (a) and (b) $N_s = 233$ and $\epsilon/J = 10^{-1}$. (c)-(d): $\sqrt{L(t)}$ for different sizes $N_s = 233$, 377 and 987 in solid green, dashed red and dotted blue respectively for $\Delta/J = 0.5$ (c) and $\Delta/J = 2.5$ (d), with $\epsilon/J = 10^{-2}$.

the non-Markovianity quantifier introduced in Eq. (1.25). Clearly, memory effects become dominant in the localised phase, but the Markovian to non-Markovian crossover does not coincides with the critical point of the Aubry-André and it is weakly affected by increasing lattice size.[4]

Interestingly, when reducing the coupling between the fermions and the impurity the rise of strong memory effects shifts towards the critical point

---

[4]Deep in the delocalised phase oscillations can be witnessed, although they result in an information backflow of several orders of magnitude lower than the information outflow making it very difficult to detect in an experimental scenario.
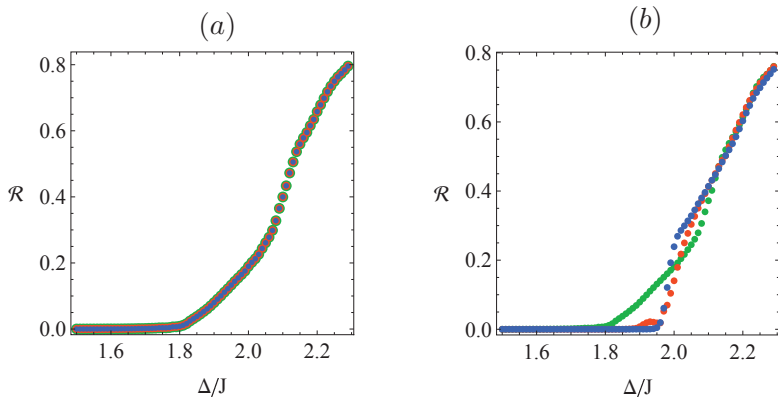
Figure 4.4: Panel (a): $\mathcal{R}$ as a function of Δ/J with $\epsilon/J = 10^{-1}$. In green, red and blue the results for $L = 233, 377$ and 987 respectively. Panel (b): $\mathcal{R}$ for a fixed size $L = 233$ with different impurity-fermions coupling, namely $\epsilon/J = 10^{-1}, 10^{-2}$ and 10^{-3} in green, red and blue respectively.

of the Aubry-André model. Panel (b) of Fig. 4.4 shows how $\mathcal{R}$ signals a sharper separation between the delocalised phase and the localised phase for weaker and weaker coupling. This evidence suggests how the memory effects witnessed by the impurity dynamics in the delocalised phase are connected to the interaction between probe and environment itself and are not only related to the phase of the environment. These memory effects are also robust and stable in the localised phase in the sense that for different couplings the ratio between information backflow and information outflow after the critical point reaches comparable values.

To conclude, in Pubblication VI we have found the information backflow experienced by the probe distinguishes the two regimes of the Aubry-André model and indeed a Markovian to non-Markovian crossover exists and it is driven by the same parameter driving the metal to insulator transition. Despite the fact that the crossover does not coincide with the critical point of the phase transition, our findings strengthen the link between memory effects and localisation and are in agreement with previous studies on non-Markovianity induced by Anderson localisation.

Chapter 5

Statistical Orthogonality Catastrophe

In 1967 P. W. Anderson introduced what he called infrared catastrophe for a Fermi gas perturbed by a local scattering potential [114]. This phenomenon has been later dubbed and referred to as Anderson Orthogonality Catastrophe (AOC). In a nutshell, the phenomenon consists in predicting a power law decay, in the system size, for the overlap between the many-body ground states of a system of non-interacting fermions with ($|\Psi_0(\epsilon)\rangle$) and without ($|\Psi_0\rangle$) an impurity potential, namely

$$F \equiv |\langle\Psi_0|\Psi_0(\epsilon)\rangle| \sim L^{-\gamma}, \tag{5.1}$$

where ϵ denotes the perturbation strength and L is the size of the system. Consequences of the AOC are witnessed by the singular behavior of excitation the energy spectra, revealed, e.g., by x-ray photoemission spectroscopy [115]. This peculiar aspect of Fermi systems has attracted a renewed interest because of the possibility to explore this phenomenon in the controllable domain of ultracold trapped gases [16, 18].

Though the AOC was first introduced to describe the effect of a local perturbation in a metallic system, recently, a new idea of a statistical orthogonality catastrophe (StOC) has been introduced for disordered insulators [116, 117]. Specifically, by studying the effect of local perturbations on the Anderson insulator and on the localised phase of the Aubry-André model, it has been found that the typical wave function overlap decays exponentially with the system size

$$F_{\text{typ}} \equiv \exp(\overline{\log F}) \sim \exp(-\alpha L). \tag{5.2}$$

The bar denotes an average over different realisations of the Fermi system: in the case of the Anderson insulator the average is taken over random realisations of the disorder while in the Aubry-André the average is taken over random realisation of the phase factor in Eq. (2.22). This Chapter summarises the findings of Publications V and VII, whose aim is to give new insight on the statistical orthogonality catastrophe.

5.1 Orthogonality events statistics

The basic difference between StOC and AOC stems from the fact that, in the former one, for certain realisations $F \simeq 1$, while for certain others $F \simeq 0$, already at finite size. This peculiarity is the reason why this form of orthogonality catastrophe has been dubbed as *statistical*.

Let us now investigate the full statistics of orthogonality events and, for this purpose, let us redefine the ground state overlap as

$$F(x, \epsilon) \equiv |\langle \Psi_0 | \Psi_0(x, \epsilon) \rangle|, \tag{5.3}$$

in order to take into account explicitly the lattice site x to which the impurity is coupled in different realisations. As a figure of merit we introduce then

$$\sigma(\epsilon) = \left\langle \frac{1}{N_s} \sum_{x=1}^{N_s} \theta(\delta - F(x, \epsilon)) \right\rangle, \tag{5.4}$$

which can be interpreted as a probability of obtaining an orthogonality event when averaging over both the position of the impurity and different realisations of the on-site potential. δ is a tolerance value within which we define two many-body wavefunctions to be *orthogonal*.

Our results show that the σ function is able to highlight the different spectral properties of the two models. For both Anderson and Aubry-André insulators, by increasing ϵ, i.e., the value of the interaction between the impurity and the Fermi system, the number of orthogonality events increases monotonically. When $\epsilon \gg \Delta$ the probability of obtaining an orthogonality event saturates to the filling factor. In Fig. 5.1 we show that the σ increases for both models when increasing the strength of the perturbation and saturates to $1/2$, which is exactly the chosen filling factor n. The striking difference, when comparing the results for the two models, is the
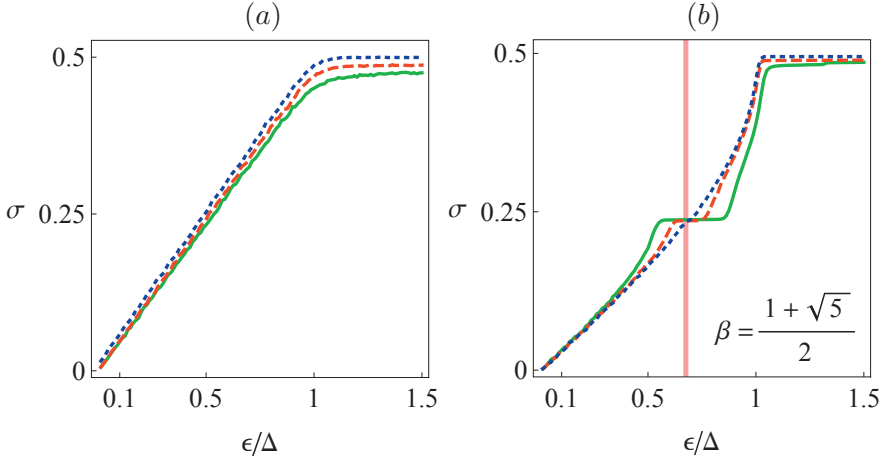
Figure 5.1: Probability σ that the ground states with and without impurity become orthogonal; the impurity is located at different lattice sites and averaged over site location and noise (or phase of potential). σ is displayed versus ϵ in units of Δ for $J/\Delta = 0.01, 0.05, 0.1$ (dotted blue, dashed red and solid green respectively). The lattice size is $N_s = 200$ and the two ground states are defined to be "orthogonal" when their overlap is less than a conventional threshold $\delta = 10^{-4}$. (a) Anderson Insulator model; (b) Aubry-André model, with β being the golden and silver ratio, respectively. The vertical line in (b) correspond to $\epsilon/\Delta = |\sin(2\pi\beta)|$.

emergence of a plateau in ϵ for the quasi-periodic potential, while in the Anderson Insulator case no particular structure is visible. This plateau seems to be of order $2J$, such as the principal energy gap of the single-particle spectrum of the Aubry-André Hamiltonian. We have found that, indeed, there is a link between the two, although not as straightforward as one could think. As explained in Refs. [116, 117] the orthogonality manifests itself when the local potential is strong enough to cause a rearrangement of particles in the two many-body ground states. When the impurity potential is switched on adiabatically, this rearrangement can be thought of as a non-local charge transfer, since the site left unoccupied in the new configuration can be very distant from the initially occupied one.

The impurity, apparently, does not change the nature of the single particle eigenstates, i.e. they are still localised, but it produces an energy shift. Qualitatively speaking, adding the impurity energy ϵ on the *occupied* site
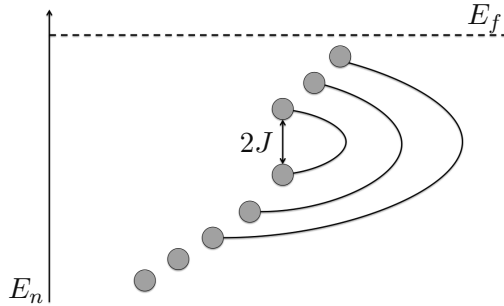
Figure 5.2: States around the principal gap are nearest neighbours and, to some extent, they are delocalised on the two sites. The closer the states are to the gap more delocalised they are.

x changes the energy of the eigenstate localised on the specific site to

$$E'_x \simeq E_x + \epsilon, \tag{5.5}$$

where E_x is the unperturbed eigenenergy. Whenever E'_x becomes greater than the energy of the first unoccupied level an *orthogonality event* occurs. This mechanism is quite straightforward and it is sufficient, in first approximation, to explain and predict the behaviour of the σ function when perturbing an Anderson Insulator.

However, because of the non-zero tunnelling, the impurity energy on site x affects the energies related to the other sites $E'_{x+1}, E'_{x+2}, ...$ In principle, also these energy shifts can generate new orthogonality events whenever the neighbour of the perturbed site is *occupied*. While it does not affect the Anderson Insulator phenomenology, this mechanism is clearly visible in the Aubry-André model. The reason relies on the fact that the eigenstates of the localised phase of the single-particle Aubry-André Hamiltonian on opposite sides of the energy gap are close in space, as predicted in [87], or more specifically are delocalised on two sites to some extent. The situation is schematically depicted in Fig. 5.2.

What happens is then that, for weak values of the perturbation, orthogonality events are obtained when the increased energy of the localised state reaches the Fermi energy of the unperturbed Hamiltonian. This mechanism is what generate orthogonality events for all the states between the principal gap and the Fermi energy. When perturbing the sites related to
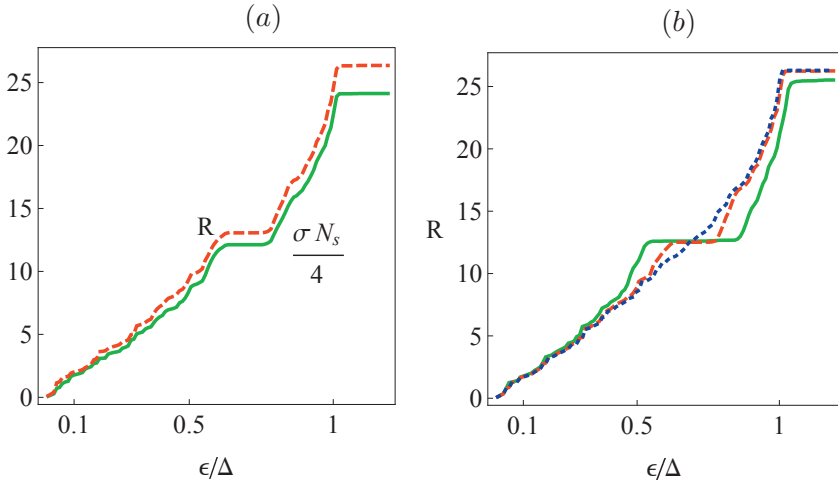
Figure 5.3: (a) The quantity R in Eq.(5.6) (dashed red) and $R \simeq \sigma N_s/4$ in Eq. (5.7) (solid green), in a system with $N_s = 200$ and $J = 0.05\Delta$ and the impurity placed in the centre of the lattice. (b) R versus ϵ/Δ, for $J/\Delta = 0.01, 0.05, 0.1$ (dotted blue, dashed red and solid green respectively).

the states directly below the principal gap the impurity affects the energy of the states localised on the neighbouring sites, that are on the other side of the gap and closer to the Fermi energy. This increase is sufficient to generate orthogonality event and the plateau starts when all the occupied sites with an occupied neighbour have generated an orthogonality event. For the states below these occupied neighbours this mechanism become unavailable and in order to generate a new orthogonality event the impurity has to match again the distance between the energy of the state and the Fermi energy, displaying then a plateau in σ. Basically, the plateau is a manifestation of the correlations in the distribution of the eigenstates, and also of the fact that the eigenstates are delocalised over two sites around the principal gap, leading to some sort of energy shortcut for generating orthogonality events.

In order to further characterise the density rearrangement induced by the impurity potential, we introduce and investigate the function

$$R_x(\epsilon) = \left\langle \sum_{j=1}^{N_s} |(j-x)\left[n(j) - \tilde{n}(j,\epsilon,x)\right]| \right\rangle_{\text{noise}}, \qquad (5.6)$$

in which $n(j) = \langle \Psi_0(\epsilon = 0)|\hat{n}_j|\Psi_0(\epsilon = 0)\rangle$ is the ground state occupation of the j-th site in absence of the impurity, and $\tilde{n}(j, \epsilon, x) = \langle \Psi_0(x, \epsilon)|\hat{n}_j|\Psi_0(x, \epsilon)\rangle$ is the ground state occupation of the j-th site in presence of an impurity at site x with interaction strength ϵ. This quantity can be interpreted, to some extent, as the average distance at which a particle is adiabatically moved as effect of the perturbation.

The transferred particle will move to the site corresponding to the lowest energy unoccupied state of the system without the impurity. This site, for random realisations of the phase, can be any lattice site with uniform probability. Therefore, for an impurity placed in the centre of the lattice, the site will be at an average distance $\sim N_s/4$. When considering the full statistics of the adiabatic transport, as a function of the perturbation potential, we can assume that the probability of an orthogonality event is equivalent to the probability to adiabatically transfer a charge, allowing us to write

$$R(\epsilon) \simeq \sigma(\epsilon)N_s/4, \tag{5.7}$$

where we have taken the impurity to be placed at site $x = N_s/2$ and consequently dropped the label x. The probability function σ is not averaged over the impurity position, but is calculated with the impurity placed at $x = N_s/2$ as well. Fig. 5.3 (a) corroborates the assumption made in (5.7). Panel (b) shows instead how the radius R behaves qualitatively like the σ function with the plateau shrinking when reducing J/Δ and saturating for strong interactions to $nN_s/4$. This result is a further confirmation that the radius of disturbance induced by the local impurity does not scale as the localisation length, which in turn is determined by the ratio J/Δ, but grows linearly with N_s.

We conclude by stressing that this analysis and the witnessed phenomenology are far from being in the thermodynamic limit. Increasing the lattice size will eventually reveal the exponential scaling of the typical fidelity, but in the regime investigated here the lattice size does not seem to play a relevant role, as shown in Fig. 5.4.
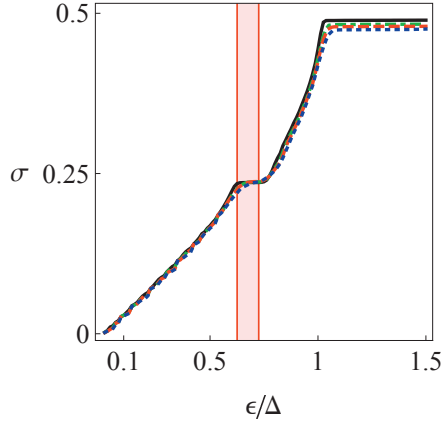
Figure 5.4: σ is displayed for different lattice size, $N_S = 200, 120, 100, 80$, in black, green, red and blue respectively with $J = 0.05\Delta$ and β being the golden ratio. The vertical red line is at $\epsilon/\Delta = |\sin(2\pi\beta)|$. The two vertical lines are at $\epsilon/\Delta = |\sin(2\pi\beta)| - J/\Delta$ and $\epsilon/\Delta = |\sin(2\pi\beta)| + J/\Delta$.

5.2 Irreversible work production and Orthogonality Catastrophe

The source behind the statistical orthogonality catastrophe can be examined from a different view point. We have outlined how, in presence of an orthogonality event, the system witnesses a change in the ground state equilibrium density, with a particle occupying a different site in the lattice in the perturbed and unperturbed configurations. Being the system localised the arrangement is due to the fact that the impurity, altering the energy of the perturbed site, makes a different state, localised on a different site, energetically favourable. This aspect of the StOC can be seen from Eq. (5.7) and is illustrated in Fig. 5.3.

We have studied how the single particle eigenstates change as function of the impurity potential. We can distinguish, as anticipated by the discussion in the previous section, two cases. In the first case the impurity perturbs an occupied site, labelled as x_0, with no nearest neighbours occupied. The orthogonality occurs whenever the state, localised at x_f, became energetically favourable to be occupied. Let's define then the energies of these two localised states as $E(x_0)$ and $E(x_f)$. The ground state density rearrange-
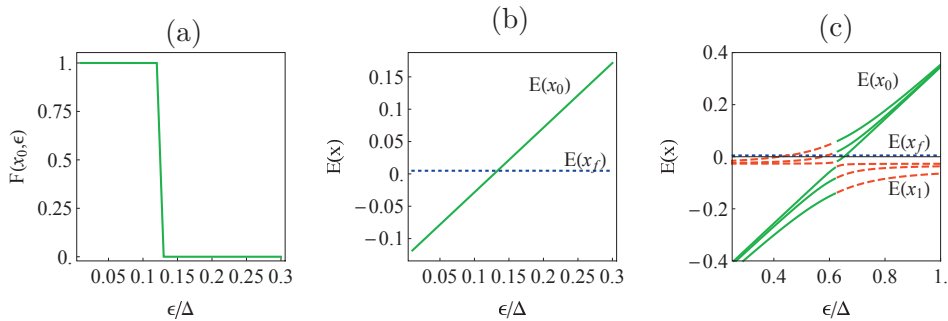
Figure 5.5: Panels (a) and (b): fidelity and level crossing when perturbing a site with no occupied neighbours. Panel (c): avoided crossing around the Fermi energy when perturbing a site with an occupied neighbour. In dashed red and solid green the energy of the states localised on the different sites. The different curves correspond to $J/\Delta = 0.1$, 0.05 and 0.01, which in terms determines the gap of the avoided crossing.

ment, or orthogonality event, is achieved when the two states, as effect of the perturbation, undergo a level crossing, i.e. $E(x_0) > E(x_f)$. Panels (a) and (b) of Fig. 5.5 summarise this explanation showing the behaviour of the ground state fidelity and the aforementioned level crossing. When the perturbed occupied site has an occupied neighbour, let's call it x_1, with $E(x_1)$ its related energy, the mechanism to generate an orthogonality event changes. As a consequence of the non-zero tunnelling the impurity modifies both $E(x_0)$ and $E(x_1)$ giving rise to an avoided crossing. Whenever one of the two is now greater than $E(x_f)$ an orthogonality event is obtained. As shown in panel (c) of Fig. 5.5, for bigger J the crossing generating the orthogonality is achieved far smaller values of the perturbation [1]. This second mechanism is the origin of the plateau like behaviour displayed for the probability of obtaining an orthogonality event in Fig. 5.1.

This description about the origin of the orthogonality catastrophe events in terms of level crossings and avoided crossings suggests to employ the same tools applied to the study of quantum phase transitions. We consider then to perform a sudden quench of the impurity potential from ϵ to $\epsilon + \delta\epsilon$. Interestingly, the irreversible work produced by such a quench is able to capture both the level crossing and the avoided crossing. In panel (a) of Fig.

---

[1] Although labelled as x_0 and x_1 it must be noticed how, close to the avoided crossing, the two states are actually delocalised on the two sites.
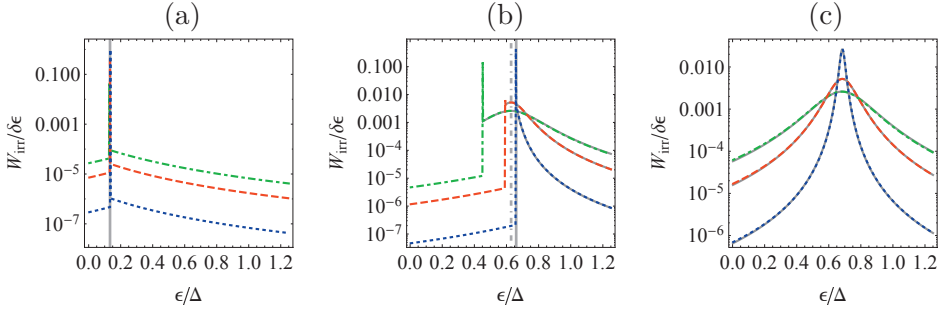
Figure 5.6: Irreversible work produced during an infinitesimal quench of the impurity potential. Panel (a), (b) and (c) correspond to the cases in which the impurity is placed in an occupied site with no occupied neighbours, an occupied neighbour, and the neighbour being x_f. $J/\Delta = 0.1$, 0.05 and 0.01 are displayed in dotdashed green, dashed red and dotted blue respectively. The gray curves in (b) and (c) are obtained plotting (5.9). The two vertical lines in (b), dashed and solid, correspond to $\epsilon = V_1 - V_0$ and $\epsilon = V_f - V_0$ respectively.

5.6 we show the irreversible work when perturbing a site with unoccupied neighbours. In this case the irreversible work is discontinuous, as expected, at the level crossing and it is unaffected by different tunnellings, as soon as we remain in the localised phase. Panel (b), corresponding to the quench of a site with an occupied neighbour, displays more interesting features. The irreversible work is discontinuous at the level crossing, between $E(x_1)$ and $E(x_f)$, while at the avoided crossing it displays a local maximum. By reducing the tunnelling J, the discontinuity moves to bigger values of the perturbation, in line with the shift seen in panel (c) of Fig. 5.5. The gray curves correspond to a fit in which we have treated the crossing as an effective two level system

$$\hat{H}_2(\epsilon) = \begin{bmatrix} V_0 + \epsilon & -J \\ -J & V_{1,} \end{bmatrix} \qquad (5.8)$$

where $V_0 = \Delta \cos(2\pi\beta x_0 + \phi)$ and $V_1 = \Delta \cos(2\pi\beta x_1 + \phi)$. With (5.8) the
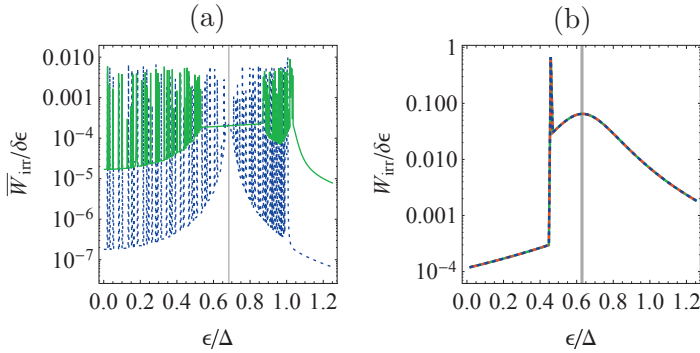
Figure 5.7: Irreversible work produced during an infinitesimal quench of the impurity potential. Panel (a): the irreversible work is averaged over the impurity position, and in solid green and dotted blue are displayed the results for $J/\Delta = 0.1$ and 0.01, respectively. Panel (b): irreversible work produced for the case in which the impurity is placed in a site with occupied neighbours for different lattice sizes, namely $N_s = 150$, 300, and 450 in green, red, and blue, respectively. The vertical lines in (a) and (b) are at $\epsilon = V_f - V_0$ and $\epsilon = V_1 - V_0$ respectively.

irreversible work for an infinitesimal quench trough (3.24) is found to be

$$W_{irr} = -\frac{\delta\epsilon^2 J^2}{\left(4J^2 + (V_0 - V_1 + \epsilon)^2\right)^{3/2}}. \tag{5.9}$$

The two-level description provides an optimal fit after the discontinuity, as depicted in panel (b) of Fig. 5.6. A particular and unique case is when the perturbed occupied site is the neighbour of x_f. In this case the irreversible work does not present any discontinuity and, at non-zero tunnelling, the irreversible work is completely described by Eq. (5.9), with $x_1 = x_f$, as displayed in panel (c) of Fig. 5.6.

When averaging over all the impurity position, the irreversible work reveals all the discontinuities related to all the possible level crossings induced in the single particle spectrum, with the development of a region with no peaks, as shown in panel (a) of Fig. 5.7. This region with no peaks is the analogous of the plateau of Fig. 5.1. By reducing the tunnelling the region shrinks and its centre coincides with $\epsilon = V_f - V_0 \approx \Delta|\sin(2\pi\beta)|$.

When increasing the lattice size we have found no noticeable changes for

the single site realisation in the range sizes considered. In panel (b) of Fig. 5.7 we see the perfect overlap obtained for increasing values of the lattice size. However, further increasing the size will eventually result in a different energy for the lowest energy unoccupied state, i.e $E(x_f)$, and on average, and for bigger sizes, it will scale at half filling as $E(x_f) \sim \frac{1}{N_s}$. Finally, increasing the lattice size leads to an increasing number of discontinuities in the irreversible work when averaging over the impurity position, signalling the increasing number of level crossings.

Concluding Remarks

In this thesis we have presented the complex and rich physics behind the topic which goes commonly under the name of quantum probing. Far from being a universal theory on quantum probes the results we have presented show how theoretical tools developed in open quantum systems theory, perturbation theory, and quantum thermodynamics can be used to design probing protocols to explore the properties of many-body systems from a novel perspective. In Chapter 1 the theory of open quantum systems, a simple derivation of the Fermi Golden Rule and the concept of work related to a quantum quench were introduced. The notion of non-Markovian dynamics was presented trough the introduction of the BLP measure, and as an example, and to prepare to the results presented later in the Thesis, the paradigmatic example of a two level system undergoing a purely dephasing dynamics was discussed.

In Chapter 2 the physical systems on which our theoretical investigations focus were presented. Such systems include the Bose-Hubbard model, describing bosons trapped in an optical lattice, Coulomb crystals, describing ions confined in anisotropic trap, Kitaev chain, describing fermionic modes with long range hopping, and the fermionic Aubry-André model, describing fermions trapped in a quasi-periodic geometry. All these models share a tight binding description and we presented some approximations which allow us to perform analytical calculations in specific regimes. It is worth mentioning that the interest in these setups arises from the fact that they are experimentally implemented in laboratories all over the world. Chapters 1 and 2 do not have the ambition to be a complete and formal analysis of the topics presented, but rather their goal is to provide the Reader with a self-consistent introduction to the basic tools necessary to better follow the results of this doctoral work.

In the following Chapters the key findings of the Publications I-VIII were presented. In Chapter 3 it was shown how a properly engineered impurity, acting as a quantum probe, can be used to perform full momentum-

resolved spectroscopy on many-body systems with a lattice-like geometry and to infer temperature via Crooks-Tasaki fluctuation theorem. In this approach the measurements are performed exclusively on the impurity, which therefore acts as a read-out device. This probing paradigm is applied to both fermionic and bosonic species. The Chapter proceeds showing how the irreversible work produced during a sudden quench in proximity of the critical point of the linear to zig-zag transition of ion Coulomb Crystals can be used to study their criticality. It is also shown how the irreversible work is, in this case, related to changes in the equilibrium positions of the ion.

In Chapter 4 we have focused our attention on the open dynamics of the impurity from an open quantum system theory perspective, trying to understand when and why it can be classified as Markovian or non-Markovian. Our goal here was to study if and how the character of the probe dynamics is related to the changing properties of the environment, e.g. when the latter one undergoes a phase transition. Our results show that a superfluid environment gives rise to a Markovian dynamics for the probe while the deep Mott insulator acts a non-Markovian reservoir. In a similar fashion we have shown how an engineered fermionic Aubry-André model can act as a Markovian and non-Markovian reservoir in the delocalised and localised regimes, respectively. Our findings substantiate the idea that a connection between memory effects and localisation exists.

Chapter 5 illustrates situations breaking the paradigm for which an impurity does not perturb sensibly a large environment. There we consider the concept of Statistical Orthogonality Catastrophe, a peculiar phenomenon arising when adding a local perturbation to localised fermionic systems. We have shown how the full statistics of orthogonality events is able to witness non trivial spectral correlations typical of the Aubry-André potential, absent in a truly disordered system. This behaviour is revealed also by quantities more accessible experimentally, such as quantifiers built on measurements of the density rearrangement induced by the impurity. We have then explored the same phenomenon from a different prospective and, using the irreversible work as a figure of merit, we have shown how the orthogonality events statistics can be described and explained trough a phenomenology of level crossings and avoided crossings.

To conclude, we have shown throughout this thesis how the impurity dynamics, intended partly as a perturbation to a large environment, is a useful tool to explore the physics of a complex environment. The theoretical tools borrowed from different fields of Physics find a natural application

in the quantum probing paradigm, which reveals itself to be an extremely versatile approach, with a wide range of applicability in terms of physical systems and properties to investigate. Consequently, there are a lot of physical phenomena that can be explored under the quantum probing umbrella. As an example, one of the following study that we will perform is the dynamical probing of the avoided crossing induced by the impurity potential in the Aubry-André model. The idea is to apply a similar procedure such in Publications III and IV in order to use the Loschmidt echo and its Fourier transform, i.e. the work statistics, to probe the avoided crossings and the resonances induced in the Fermi lattice by the immersed impurity.

The results of this research work also suggest to apply a similar methodology to achieve different goals. If here the task was to learn about the complex environment, by means of impurities and perturbation potentials, the next step is to use the same ingredients to manipulate, at will, the quantum complex system itself or the open dynamics of the probe. Critical regions are already been proven to be an optimal operational regime for efficient quantum thermal machines. However, critical-like phenomena driven by impurities have not been yet widely studied in this framework. At the same time, the possibility of tailoring localised energy states in large localised environments, by means of an impurity potential, suggest the design of a novel architecture for quantum information processing. Another direction could be to use impurity potentials and properly engineered time-dependent couplings to perform cooling protocols. These future directions harvest the experience developed throughout this thesis in the field of quantum probing and direct it into the manipulation and engineering of open quantum systems and complex environments.

Bibliography

[1] T. H. Johnson, F. Cosco, M. T. Mitchison, D. Jaksch, and S. R. Clark, Phys. Rev. A **93**, 053619 (2016).

[2] F. Cosco, M. Borrelli, F. Plastina, and S. Maniscalco, Phys. Rev. A **95**, 053620 (2017).

[3] F. Cosco, M. Borrelli, P. Silvi, S. Maniscalco, and G. De Chiara, Phys. Rev. A **95**, 063615 (2017).

[4] F. Cosco, M. Borrelli, J. J. Mendoza-Arenas, F. Plastina, D. Jaksch, and S. Maniscalco, Phys. Rev. A **97**, 040101 (2018).

[5] F. Cosco, M. Borrelli, E.-M. Laine, S. Pascazio, A. Scardicchio, and S. Maniscalco, New Journal of Physics **20**, 073041 (2018).

[6] F. Cosco and S. Maniscalco, Phys. Rev. A **98**, 053608 (2018).

[7] F. Cosco, arXiv:1809.01855 (2018).

[8] F. Cosco, M. Borrelli, F. Plastina, and S. Maniscalco, arXiv:1811.01939 (2018).

[9] T. H. Johnson, S. R. Clark, M. Bruderer, and D. Jaksch, Phys. Rev. A **84**, 023617 (2011).

[10] A. Kantian, U. Schollwöck, and T. Giamarchi, Phys. Rev. Lett. **115**, 165301 (2015).

[11] M. T. Mitchison, T. H. Johnson, and D. Jaksch, Phys. Rev. A **94**, 063618 (2016).

[12] R. Dorner, S. R. Clark, L. Heaney, R. Fazio, J. Goold, and V. Vedral, Phys. Rev. Lett. **110**, 230601 (2013).

[13] D. Hangleiter, M. T. Mitchison, T. H. Johnson, M. Bruderer, M. B. Plenio, and D. Jaksch, Phys. Rev. A **91**, 013611 (2015).

[14] A. Abdelrahman, O. Khosravani, M. Gessner, A. Buchleitner, H. P. Breuer, D. Gorman, R. Masuda, T. Pruttivarasin, M. Ramm, P. Schindler, et al., Nature Communications **8**, 15712 EP (2017).

[15] A. Recati, P. O. Fedichev, W. Zwerger, J. von Delft, and P. Zoller, Phys. Rev. Lett. **94**, 040404 (2005).

[16] J. Goold, T. Fogarty, N. Lo Gullo, M. Paternostro, and T. Busch, Phys. Rev. A **84**, 063632 (2011).

[17] M. Knap, A. Shashi, Y. Nishida, A. Imambekov, D. A. Abanin, and E. Demler, Phys. Rev. X **2**, 041020 (2012).

[18] A. Sindona, J. Goold, N. Lo Gullo, S. Lorenzo, and F. Plastina, Phys. Rev. Lett. **111**, 165303 (2013).

[19] A. Sindona, J. Goold, N. L. Gullo, and F. Plastina, New Journal of Physics **16**, 045013 (2014).

[20] M. Schiró and A. Mitra, Phys. Rev. Lett. **112**, 246401 (2014).

[21] S. Lorenzo, F. Lombardo, F. Ciccarello, and G. M. Palma, Scientific Reports **7**, 42729 (2017).

[22] J. Nokkala, F. Galve, R. Zambrini, S. Maniscalco, and J. Piilo, Scientific Reports **6**, 26861 EP (2016).

[23] S. Cialdi, C. Porto, D. Cipriani, S. Olivares, and M. G. A. Paris, Phys. Rev. A **93**, 043805 (2016).

[24] P. Haikka, J. Goold, S. McEndoo, F. Plastina, and S. Maniscalco, Phys. Rev. A **85**, 060101 (2012).

[25] M. Borrelli, P. Haikka, G. De Chiara, and S. Maniscalco, Phys. Rev. A **88**, 010101 (2013).

[26] T. J. G. Apollaro, G. Francica, D. Giuliano, G. Falcone, G. M. Palma, and F. Plastina, Phys. Rev. B **96**, 155145 (2017).

[27] C. Benedetti, F. Salari Sehdaran, M. H. Zandi, and M. G. A. Paris, Phys. Rev. A **97**, 012126 (2018).

[28] P. Haikka, S. McEndoo, and S. Maniscalco, Phys. Rev. A **87**, 012127 (2013).

[29] D. Tamascelli, C. Benedetti, S. Olivares, and M. G. A. Paris, Phys. Rev. A **94**, 042129 (2016).

[30] M. A. C. Rossi and M. G. A. Paris, Phys. Rev. A **92**, 010302 (2015).

[31] M. Bina, F. Grasselli, and M. G. A. Paris, Phys. Rev. A **97**, 012125 (2018).

[32] J. Catani, G. Barontini, G. Lamporesi, F. Rabatti, G. Thalhammer, F. Minardi, S. Stringari, and M. Inguscio, Phys. Rev. Lett. **103**, 140401 (2009).

[33] C. Weitenberg, M. Endres, J. F. Sherson, M. Cheneau, P. Schauß, T. Fukuhara, I. Bloch, and S. Kuhr, Nature **471**, 319 EP (2011).

[34] E. Haller, J. Hudson, A. Kelly, D. A. Cotta, B. Peaudecerf, G. D. Bruce, and S. Kuhr, Nature Physics **11**, 738 EP (2015).

[35] M. Cetina, M. Jag, R. S. Lous, I. Fritsche, J. T. M. Walraven, R. Grimm, J. Levinsen, M. M. Parish, R. Schmidt, M. Knap, et al., Science **354**, 96 (2016).

[36] H. P. Breuer and F. Petruccione, *The theory of open quantum systems* (Oxford University Press, 2002).

[37] G. Lindblad, Communications in Mathematical Physics **48**, 119 (1976).

[38] V. Gorini, A. Kossakowski, and E. C. G. Sudarshan, Journal of Mathematical Physics **17**, 821 (1976).

[39] M. M. Wolf and J. I. Cirac, Communications in Mathematical Physics **279**, 147 (2008).

[40] A. Rivas, S. F. Huelga, and M. B. Plenio, Phys. Rev. Lett. **105**, 050403 (2010).

[41] S. Luo, S. Fu, and H. Song, Phys. Rev. A **86**, 044101 (2012).

[42] S. Lorenzo, F. Plastina, and M. Paternostro, Phys. Rev. A **88**, 020102 (2013).

[43] N. Lo Gullo, I. Sinayskiy, T. Busch, and F. Petruccione, arXiv:1401.1126 (2014).

[44] B. Bylicka, D. Chruściński, and S. Maniscalco, Scientific Reports **4**, 5720 EP (2014).

[45] F. A. Pollock, C. Rodríguez-Rosario, T. Frauenheim, M. Paternostro, and K. Modi, Phys. Rev. Lett. **120**, 040405 (2018).

[46] H.-P. Breuer, E.-M. Laine, and J. Piilo, Phys. Rev. Lett. **103**, 210401 (2009).

[47] H.-P. Breuer, E.-M. Laine, J. Piilo, and B. Vacchini, Rev. Mod. Phys. **88**, 021002 (2016).

[48] S. Wißmann, A. Karlsson, E.-M. Laine, J. Piilo, and H.-P. Breuer, Phys. Rev. A **86**, 062108 (2012).

[49] E. Fermi, *Nuclear Physics, Notes compiled by J. Orear, A. H. Rosenfeld, and R. A. Schluter* (The University of Chicago Press, Chicago, 1950).

[50] J. Dereziński and R. Früboes, *Fermi Golden Rule and Open Quantum Systems* (Springer Berlin Heidelberg, Berlin, Heidelberg, 2006), pp. 67–116, ISBN 978-3-540-33967-0.

[51] P. Talkner, E. Lutz, and P. Hänggi, Phys. Rev. E **75**, 050102 (2007).

[52] G. E. Crooks, Phys. Rev. E **60**, 2721 (1999).

[53] H. Tasaki, arXiv:cond-mat/0009244 (2000).

[54] F. Plastina, A. Alecce, T. J. G. Apollaro, G. Falcone, G. Francica, F. Galve, N. Lo Gullo, and R. Zambrini, Phys. Rev. Lett. **113**, 260601 (2014).

[55] C. Jarzynski, Phys. Rev. Lett. **78**, 2690 (1997).

[56] J. Goold, F. Plastina, A. Gambassi, and A. Silva, arXiv:1804.02805 (2018).

[57] D. Jaksch, C. Bruder, J. I. Cirac, C. W. Gardiner, and P. Zoller, Phys. Rev. Lett. **81**, 3108 (1998).

[58] M. Greiner, O. Mandel, T. Esslinger, T. W. Hänsch, and I. Bloch, Nature **415**, 39 EP (2002).

[59] S. R. Clark and D. Jaksch, Phys. Rev. A **70**, 043612 (2004).

[60] M. A. Cazalilla, R. Citro, T. Giamarchi, E. Orignac, and M. Rigol, Rev. Mod. Phys. **83**, 1405 (2011).

[61] M. A. Cazalilla, Phys. Rev. A **67**, 053606 (2003).

[62] B. Paredes, A. Widera, V. Murg, O. Mandel, S. Fölling, I. Cirac, G. V. Shlyapnikov, T. W. Hänsch, and I. Bloch, Nature **429**, 277 EP (2004).

[63] N. N. Bogoliubov, J. Phys. USSR **11**, 23 (1947).

[64] D. van Oosten, P. van der Straten, and H. T. C. Stoof, Phys. Rev. A **63**, 053601 (2001).

[65] K. Burnett, M. Edwards, C. W. Clark, and M. Shotter, Journal of Physics B: Atomic, Molecular and Optical Physics **35**, 1671 (2002).

[66] A. M. Rey, K. Burnett, R. Roth, M. Edwards, C. J. Williams, and C. W. Clark, Journal of Physics B: Atomic, Molecular and Optical Physics **36**, 825 (2003).

[67] P. Barmettler, D. Poletti, M. Cheneau, and C. Kollath, Phys. Rev. A **85**, 053625 (2012).

[68] C. D. Batista and G. Ortiz, Phys. Rev. Lett. **86**, 1082 (2001).

[69] D. H. E. Dubin and T. M. O'Neil, Rev. Mod. Phys. **71**, 87 (1999).

[70] D. H. E. Dubin, Phys. Rev. Lett. **71**, 2753 (1993).

[71] S. Fishman, G. De Chiara, T. Calarco, and G. Morigi, Phys. Rev. B **77**, 064111 (2008).

[72] E. Shimshoni, G. Morigi, and S. Fishman, Phys. Rev. Lett. **106**, 010401 (2011).

[73] P. Silvi, T. Calarco, G. Morigi, and S. Montangero, Phys. Rev. B **89**, 094103 (2014).

[74] P. Silvi, G. De Chiara, T. Calarco, G. Morigi, and S. Montangero, Annalen der Physik **525**, 827 (2013).

[75] D. Podolsky, E. Shimshoni, P. Silvi, S. Montangero, T. Calarco, G. Morigi, and S. Fishman, Phys. Rev. B **89**, 214408 (2014).

[76] D. Vodola, L. Lepori, E. Ercolessi, A. V. Gorshkov, and G. Pupillo, Phys. Rev. Lett. **113**, 156402 (2014).

[77] D. Vodola, L. Lepori, E. Ercolessi, and G. Pupillo, New Journal of Physics **18**, 015001 (2016).

[78] A. S. Buyskikh, M. Fagotti, J. Schachenmayer, F. Essler, and A. J. Daley, Phys. Rev. A **93**, 053620 (2016).

[79] J. W. Britton, B. C. Sawyer, A. C. Keith, C. C. J. Wang, J. K. Freericks, H. Uys, M. J. Biercuk, and J. J. Bollinger, Nature **484**, 489 EP (2012).

[80] P. Richerme, Z.-X. Gong, A. Lee, C. Senko, J. Smith, M. Foss-Feig, S. Michalakis, A. V. Gorshkov, and C. Monroe, Nature **511**, 198 EP (2014).

[81] C. Schneider, D. Porras, and T. Schaetz, Reports on Progress in Physics **75**, 024401 (2012).

[82] L. Sanchez-Palencia and M. Lewenstein, Nature Physics **6**, 87 EP (2010).

[83] M. Schreiber, S. S. Hodgman, P. Bordia, H. P. Lüschen, M. H. Fischer, R. Vosk, E. Altman, U. Schneider, and I. Bloch, Science **349**, 842 (2015).

[84] H. P. Lüschen, P. Bordia, S. Scherg, F. Alet, E. Altman, U. Schneider, and I. Bloch, Phys. Rev. Lett. **119**, 260401 (2017).

[85] S. Aubry and G. André, Ann. Israel Phys. Soc **3**, 18 (1980).

[86] J. B. Sokoloff, Phys. Rev. B **23**, 6422 (1981).

[87] D. J. Thouless and Q. Niu, Journal of Physics A: Mathematical and General **16**, 1911 (1983).

[88] M. Modugno, New Journal of Physics **11**, 033023 (2009).

[89] S. Y. Jitomirskaya, Annals of Mathematics **150**, 1159 (1999).

[90] C. Schori, T. Stöferle, H. Moritz, M. Köhl, and T. Esslinger, Phys. Rev. Lett. **93**, 240402 (2004).

[91] P. T. Ernst, S. Götze, J. S. Krauser, K. Pyka, D.-S. Lühmann, D. Pfannkuche, and K. Sengstock, Nature Physics **6**, 56 EP (2009).

[92] R. Walters, G. Cotugno, T. H. Johnson, S. R. Clark, and D. Jaksch, Phys. Rev. A **87**, 043613 (2013).

[93] M. Brunelli, S. Olivares, M. Paternostro, and M. G. A. Paris, Phys. Rev. A **86**, 012125 (2012).

[94] S. Jevtic, D. Newman, T. Rudolph, and T. M. Stace, Phys. Rev. A **91**, 012331 (2015).

[95] L. A. Correa, M. Mehboudi, G. Adesso, and A. Sanpera, Phys. Rev. Lett. **114**, 220405 (2015).

[96] L. Mancino, M. Sbroscia, I. Gianani, E. Roccia, and M. Barbieri, Phys. Rev. Lett. **118**, 130502 (2017).

[97] L. Seveso and M. G. A. Paris, Phys. Rev. A **97**, 032129 (2018).

[98] L. Mazzola, G. De Chiara, and M. Paternostro, Phys. Rev. Lett. **110**, 230602 (2013).

[99] R. Dorner, J. Goold, C. Cormick, M. Paternostro, and V. Vedral, Phys. Rev. Lett. **109**, 160601 (2012).

[100] E. Mascarenhas, H. Bragança, R. Dorner, M. França Santos, V. Vedral, K. Modi, and J. Goold, Phys. Rev. E **89**, 062103 (2014).

[101] S. Sharma and A. Dutta, Phys. Rev. E **92**, 022108 (2015).

[102] F. A. Bayocboc and F. N. C. Paraan, Phys. Rev. E **92**, 032142 (2015).

[103] A. Bayat, T. J. G. Apollaro, S. Paganelli, G. De Chiara, H. Johannesson, S. Bose, and P. Sodano, Phys. Rev. B **93**, 201106 (2016).

[104] S. Paganelli and T. J. Apollaro, International Journal of Modern Physics B p. 1750065 (2016).

[105] R. P. Feynman, Phys. Rev. **56**, 340 (1939).

[106] H. Kaufmann, S. Ulm, G. Jacob, U. Poschinger, H. Landa, A. Retzker, M. B. Plenio, and F. Schmidt-Kaler, Phys. Rev. Lett. **109**, 263003 (2012).

[107] K. Pyka, J. Keller, H. L. Partner, R. Nigmatullin, T. Burgermeister, D. M. Meier, K. Kuhlmann, A. Retzker, M. B. Plenio, W. H. Zurek, et al., Nature Communications **4**, 2291 EP (2013).

[108] S. Ulm, J. Roßnagel, G. Jacob, C. Degünther, S. T. Dawkins, U. G. Poschinger, R. Nigmatullin, A. Retzker, M. B. Plenio, F. Schmidt-Kaler, et al., Nature Communications **4**, 2290 EP (2013).

[109] J. Roßnagel, S. T. Dawkins, K. N. Tolazzi, O. Abah, E. Lutz, F. Schmidt-Kaler, and K. Singer, Science **352**, 325 (2016).

[110] M. Bruderer and D. Jaksch, New Journal of Physics **8**, 87 (2006).

[111] S. Vardhan, G. De Tomasi, M. Heyl, E. J. Heller, and F. Pollmann, Phys. Rev. Lett. **119**, 016802 (2017).

[112] L. S. Levitov and G. B. Lesovik, Soviet Journal of Experimental and Theoretical Physics Letters **58**, 230 (1993).

[113] I. Klich (Springer Netherlands, Dordrecht, 2003), pp. 397–402, ISBN 978-94-010-0089-5.

[114] P. W. Anderson, Phys. Rev. Lett. **18**, 1049 (1967).

[115] Y. Tanabe and K. Ohtaka, Phys. Rev. B **32**, 2036 (1985).

[116] V. Khemani, R. Nandkishore, and S. Sondhi, Nature Physics **11**, 560 (2015).

[117] D.-L. Deng, J. H. Pixley, X. Li, and S. Das Sarma, Phys. Rev. B **92**, 220201 (2015).

Annales Universitatis Turkuensis

UNIVERSITY OF TURKU